INFORMATION TO USERS

This manuscript has been reproduced from the microfilm master. UMI films the text directly from the original or copy submitted. Thus, some thesis and dissertation copies are in typewriter face, while others may be from any type of computer printer.

The quality of this reproduction is dependent upon the quality of the copy submitted. Broken or indistinct print, colored or poor quality illustrations and photographs, print bleedthrough, substandard margins, and improper alignment can adversely affect reproduction.

In the unlikely event that the author did not send UMI a complete manuscript and there are missing pages, these will be noted. Also, if unauthorized copyright material had to be removed, a note will indicate the deletion.

Oversize materials (e.g., maps, drawings, charts) are reproduced by sectioning the original, beginning at the upper left-hand corner and continuing from left to right in equal sections with small overlaps.

Photographs included in the original manuscript have been reproduced xerographically in this copy. Higher quality 6" x 9" black and white photographic prints are available for any photographs or illustrations appearing in this copy for an additional charge. Contact UMI directly to order.

ProQuest Information and Learning
300 North Zeeb Road, Ann Arbor, MI 48106-1346 USA
800-521-0600

Reproduced with permission of the copyright owner. Further reproduction prohibited without permission.

Reproduced with permission of the copyright owner. Further reproduction prohibited without permission.

VALIDATION OF ELECTRONIC PACKAGE RELIABILITY USING SPECKLE INTERFEROMETRY

A THESIS

Presented to the Department of Mechanical Engineering

California State University, Long Beach

In Partial Fulfillment

of the Requirements for the Degree

Master of Science

By Kevin Joseph Cote

B.S., 1996, California State University, Fullerton

December 2000

Reproduced with permission of the copyright owner. Further reproduction prohibited without permission.

UMI Number: 1403513

UMI®

UMI Microform 1403513
Copyright 2001 by Bell & Howell Information and Learning Company.
All rights reserved. This microform edition is protected against
unauthorized copying under Title 17, United States Code.

Bell & Howell Information and Learning Company
300 North Zeeb Road
P.O. Box 1346
Ann Arbor, MI 48106-1346

Reproduced with permission of the copyright owner. Further reproduction prohibited without permission.

WE, THE UNDERSIGNED MEMBERS OF THE COMMITTEE,

HAVE APPROVED THIS THESIS

VALIDATION OF ELECTRONIC PACKAGE RELIABILITY USING

SPECKLE INTERFEROMETRY

By

Kevin Joseph Cote

COMMITTEE MEMBERS

Hsien-Yang Yeh, Ph.D. (Chair) Mechanical Engineering

Hamid Rahai, Ph.D. Mechanical Engineering

Min-Ten Jahn, Ph.D. Mechanical Engineering

ACCEPTED AND APPROVED ON BEHALF OF THE UNIVERSITY

Leonardo Perez y Perez, Ph.D.
Department Chair, Department of Mechanical Engineering

California State University, Long Beach

December 2000

Reproduced with permission of the copyright owner. Further reproduction prohibited without permission.

ABSTRACT

VALIDATION OF ELECTRONIC PACKAGE RELIABILITY USING SPECKLE INTERFEROMETRY

By

Kevin Joseph Cote

December 2000

In-situ measurements were performed on a land grid array electronic package using Electronic Speckle Pattern Interferometry. Unlike other whole field deformation techniques such as Moiré Interferometry, which is typically used by the electronic packaging industry, Electronic Speckle Pattern Interferometry does not require a thin film grating to be applied to the specimen. Moreover, this grating can often skew the measurements if not applied properly.

Due to coefficient of thermal expansion mismatches between the package and printed circuit board, creep shear strains developed in the 63/37 SnPb solder. When thermally loaded, these creep shear strains develop cracks in the joint leading to Mode II failure. A single thermal half cycle from 25^0C to 125^0C was applied to a specimen to simulate the fatigue life of the solder joints undergoing thermal loading and the resulting strains were entered into the Engelmaier reliability prediction model for 63/37 SnPb solder. An equivalent finite element model was developed to validate these results using bilinear and multilinear coefficient of thermal expansion and

Reproduced with permission of the copyright owner. Further reproduction prohibited without permission.

temperature dependent modulus properties. The experimental results yielded 0.59% strain per cycle with 7485 cycles to failure while the bilinear and multilinear models yield 0.682% and 0.642% strain, respectively leading to 5880 and 6503 cycles to failure.

Reproduced with permission of the copyright owner. Further reproduction prohibited without permission.

TABLE OF CONTENTS

Page

LIST OF TABLES vi

LIST OF FIGURES vii

LIST OF NOMENCLATURE ix

CHAPTER

1. INTRODUCTION 1

2. ELECTRONIC SPECKLE PATTERN INTERFEROMETRY 8

3. SUBSTRATE MATERIALS CHARACTERIZATION 17

4. EQUIVALENT FINITE ELEMENT MODEL 24

5. CONCLUSION 37

APPENDICES

A. EXPERIMENTAL MATERIAL PROPERTIES 42

B. RELIABILITY MODELS FOR CREEP STRAIN ANALYSIS 50

C. ANSYS INPUT DECK FILES 59

BIBLIOGRAPHY 81

Reproduced with permission of the copyright owner. Further reproduction prohibited without permission.

LIST OF TABLES

TABLE Page

1. CTE of Various Materials Used in Electronic Packaging 3

2. Calculated Temperature Dependent CTE Value of Sample Number One . . . 20

3. Experimental and Numerical Reliability Results 39

4. Measured CTE Values of BT, Sample #1 43

5. Measured CTE Values of BT, Sample #2 43

6. Measured CTE Values of BT, Sample #3 44

7. Measured CTE Values of Copper, Sample #1 45

8. Measured CTE Values of Copper, Sample #2 46

9. Measured CTE Values of Copper, Sample #3 46

Reproduced with permission of the copyright owner. Further reproduction prohibited without permission.

LIST OF FIGURES

FIGURE Page

1. Thermal response of half of idealized structure 4

2. Approximate stress model for LGA solder joint, undeformed and deformed . 5

3. Schematic of force-displacement hysteresis for a solder 6

4. ESPI setup for strain measurements 9

5. Light waves for both non-deformed and deformed patterns 10

6. Speckle pattern of both non-deformed and deformed object 10

7. Resulting difference between original pattern and deformed pattern 11

8. Schematic of LGA test assembly 14

9. Fringe pattern from speckle pattern correlation between 125^0C and 25^0C . . 15

10. Calculated strain in the package assembly due to thermal loading 15

11. Material set for CTE and modulus measurements 17

12. Experimental setup for CTE measurements 18

13. Graph of strain versus temperature result for BT 20

14. Dog bone specimen used to determine modulus 21

15. Experimental setup for modulus testing 22

16. Experimental data and bilinear model of BT resin at the three temperatures . 23

17. Difference of instantaneous CTE and effective CTE 26

18. Method for determining the bilinear fit modulus from experimental data . . 27

19. Format for a multilinear isotropic hardening material property 28

Reproduced with permission of the copyright owner. Further reproduction prohibited without permission.

FIGURE Page

20. Position vectors and motion of a deforming body 29

21. Stress relaxation and creep phenomenon 31

22. Plane183 two-dimensional eight node structural element 33

23. Final half symmetry mesh pattern of 5mm LGA package 33

24. Elastic, creep, and total shear strain plotted versus time, multilinear 34

25. Hysteresis loop of solder joint, multilinear 35

26. Elastic, creep, and total shear strain plotted versus time, bilinear 36

27. Hysteresis loop of solder joint, bilinear 36

28. Measured strain values versus temperature for BT resin 45

29. Measured strain value versus temperature for copper material 47

30. Experimental results and bilinear fit of BT resin 48

31. Experimental temperature dependent and bilinear fit of copper 49

Reproduced with permission of the copyright owner. Further reproduction prohibited without permission.

LIST OF NOMENCLATURE

Sn	Tin
Pb	Lead
PWB	Printed Wiring Board
PCB	Printed Circuit Board
LGA	Land Grid Array
Au	Gold
SMT	Surface Mount Technology
CSP	Chip Scale Package
CTE	Coefficient of Thermal Expansion
ESPI	Electronic Speckle Pattern Interferometry
FEA	Finite Element Analysis
BT	Bismaleimide Triazine
$\{\sigma\}$	Stress Vector
$[D]$	Elasticity Matrix
$\{\varepsilon\}$	Strain Vector
α	Coefficient of Thermal Expansion
T	Temperature
E	Young's Modulus
ν	Poisson's Ratio

Reproduced with permission of the copyright owner. Further reproduction prohibited without permission.

G	Shear Modulus
[I]	Identity Matrix
[R]	Rotation Matrix
[U]	Shaper Change Matrix
λ	Eigenvalue
{e}	Eigenvector
$d\gamma/dt$	Creep Strain Rate
H	Activation Energy
R	Universal Gas Constant
APDL	ANSYS Parametric Design Language
ppm	Parts Per Million
F	Proportionality Factor
n_f	Uncorrected Cycles to Fail
c	Fatigue Ductility Exponent
K_l	Life Correction Factor
K_r	Reliability Correction Factor
α'	Weibull Scale Parameter
β	Weibull Shape Parameter
N_f	Corrected Cycles to Fail

Reproduced with permission of the copyright owner. Further reproduction prohibited without permission.

CHAPTER 1

INTRODUCTION

Electronic packaging is the technology of packaging electronic equipment which includes the interconnection of electronic components into printed wiring boards (PWBs) and the interconnection of printed wiring boards to electronic assemblies [1]. Due to the increased use of computers and electronics in all aspects of our lives, increasing performance of electronic packaging configurations without the increasing cost is becoming a major thrust of the electronics industry.

Due to differences in materials and configuration requiring a different analytical approach, an electronic package configuration is frequently broken down into three levels [2]. The first level or component level provides a method for attaching and interconnecting a silicon die to the substrate of printed circuit board (PCB). For the land grid array (LGA) package used in this thesis, this interconnect is accomplished using gold (Au) wire bonds from the die to the PCB.

The second level or module level packaging interconnects components to the next level of packaging, which is the PWB. This can be accomplished either using through-hole or surface mount technology (SMT). The latter is used for the LGA package. With SMT, solder joints are generated by screen printing a solder paste material onto the PWB. The LGA package is then placed on top of the solder paste and the assembly is reflowed in a furnace to form the solder joints.

Reproduced with permission of the copyright owner. Further reproduction prohibited without permission.

The third and final level or chassis level package includes support rails to which the modules are mounted, and a motherboard with connectors that provide electrical interconnection to other modules and the main chassis connectors. For this thesis however, the chassis level will not be considered due to its irrelevance to the package solder joint reliability.

The LGA is classified as a chip scale package (CSP), meaning the size of the silicon die is slightly smaller than the size of the package. CSP packages are used in applications were the overall size of the system is critical. In the case of the LGA, it is used as a transmit/receive chip in cellular phones. The structure of the LGA package is comprised of a two metal layer circuit board with a silicon die attached via a non-conductive epoxy. The die is protected from the environment by a mold cap. As with any new packaging technology, the mechanical reliability of the package must be analyzed. For the LGA package this is critical due to the relative size of the solder joint compared to the size of the package.

Electronic packages are constructed of many different materials that have different coefficient of thermal expansion (CTE) values. The CTE is the change in linear dimension per unit length per degree change of the bulk material temperature [3]. Due to of the variations in CTE of each material, when the package assembly is subjected to thermal loading, strains develop in the solder joints. To quantify these strains, thermal cycling is used to determine the solder joint reliability of the package. This occurs naturally in the real world application such as when a device is powered up and then shut off repeatedly over time.

Reproduced with permission of the copyright owner. Further reproduction prohibited without permission.

Table 1 lists the CTE values of materials commoly used in electronic packaging. The differential expansion, or mismatch, must be accommodated by the various elements. Packages are subject to two types of heat exposure: process cycles, which are often high in temperature but few in number; and operation cycles, which are numerous but less extreme. This thesis deals only with the latter. The assumption being that the structure has survived manufacturing and burn-in stresses. If any of the solder joints are unable to repeatedly bear their share of the system mismatch over the lifetime, the joints will fracture, prematurely terminating functionality of the package. This failure is known as thermal fatigue.

TABLE 1. CTE of Various Materials Used in Electronic Packaging

Material	CTE (10^{-6} per degree Celsius at 25°)
Alloy 42	6.0
Titanium	10.0
Iron	12.0
Gold	14.2
Nickel	13.0-15.0
Gold-tin eutectic	16.0
Copper	16.0-18.0
Silver	19.0
Lead-tin eutectic	21.0
Silicon	2.8
Alumina	6.7
Epoxy Glass	11.0-15.0
Polyimides	40.0-50.0
Epoxies	60.0-80.0

Component geometries that are potential candidates for themal fatigue can usually be generalized as two relatively rigid elements (typically a chip or chip carrier; substrate, printed wiring board, or heat sink), joined by a softer interconnection or array of interconnections, solder joints [4]. By virtue of geometry and materials, the

Reproduced with permission of the copyright owner. Further reproduction prohibited without permission.

interconnection can vary in softness from very compliant, like the LGA solder joint, to relatively stiff. In the former case most of the thermal mismatch is borne by the interconnection, while the latter, the force is evenly distributed throughout the region. A simplified model of the LGA package can be shown as two dissimilar materials connected via a compliant solder joint. When a thermal load is applied to the model, the materials expand at different rates and the mismatch is absorbed by the solder joint.

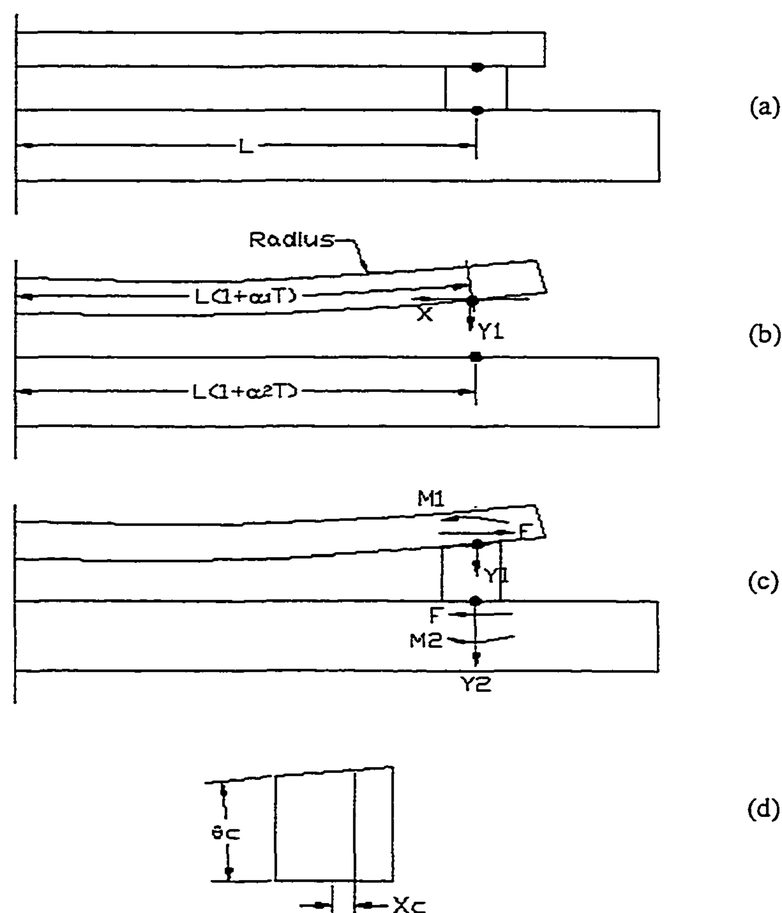

FIGURE 1. Thermal response of half of idealized structure. (a) Room temperature. (b) elevated temperature beams contrained. (c) constrained state. (d) magnified view of solder joint.

Reproduced with permission of the copyright owner. Further reproduction prohibited without permission.

To obtain an approximate solution, the same short beam shown in figure 1 may be utilized to develop approximate stresses in the solder joint. Details of the model assumptions are shown in Figure 2 for both undeformed and deformed. The weakest assumption underlying the idealization is that every plane horizontal cross section in the joint remains plane during the deformation [5]. However, it is useful to keep these models in mind when verifying FEM results.

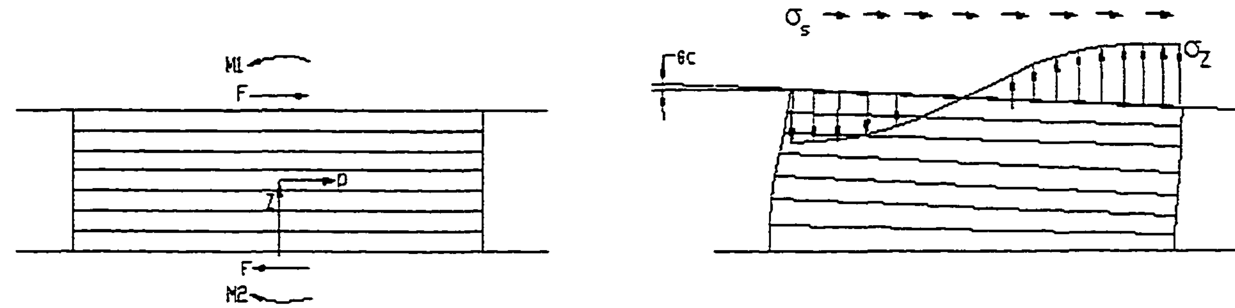

FIGURE 2. Approximate stress model for LGA solder joint, undeformed and deformed.

The terminal is segemented into a stack of rectangular plates, each of which may shear, stretch, or compress but always remain plane. Nonlinearity can be approximated by assuming a single work-hardening coefficient.

Operating at an absolute temperature over half the melting point of 183^{0}C, the solder joint's mechanical behavior does not only depend upon the applied force or displacement field but also upon time and temperature. Measured properties of bulk solder show that flow properties alter drastically with temperature. In addition, a set of interactive creep mechanisms come into play, each with its own stress, temperature, and

Reproduced with permission of the copyright owner. Further reproduction prohibited without permission.

grain size dependencies. Creep is the time-dependent deformation of a material under constant mechanical stress and temperature [6]. Although high-temperature solder deformation is complex, one may describe soft solder as being relatively rigid at low temperatures and dramatically softened by 100°C.

At low temperatures the plates in figure two diverge only slightly because of small quasi-elastic deformation of the terminals. At higher temperatures the plates tend to straighten as the solder weakens, and by 120°C there is no remaining bending, and presumably no constraint to free plate expansion. Figure 3 is a schematic representation of the steady-state hysteresis loop in comparison to high and low temperature isothermal curves of a typical solder joint which is developed after several "break-in" cycles. Thermal wearout is a relatively long-term phenomenon. Due to this condition, the behavior prior to steady-state conditions is seldom of importance.

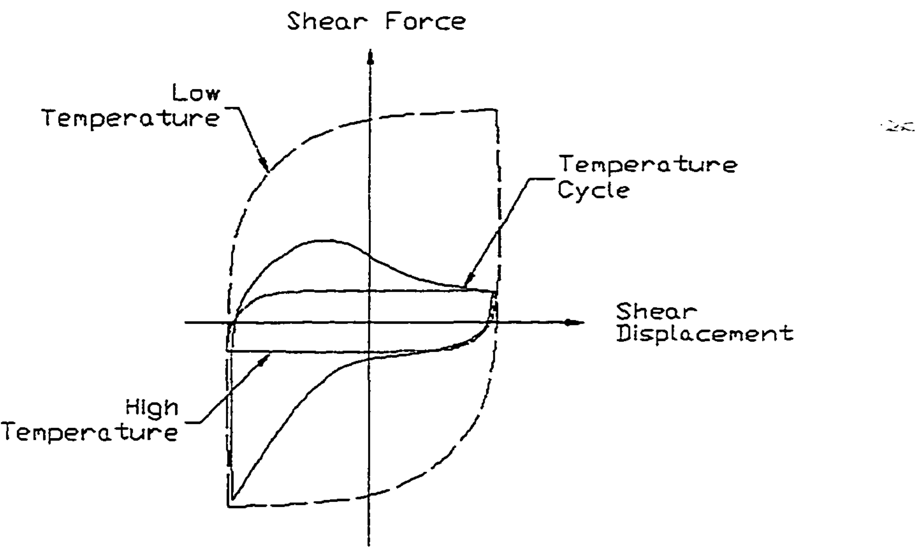

FIGURE 3. Schematic of force-displacement hysteresis for a solder.

Reproduced with permission of the copyright owner. Further reproduction prohibited without permission.

Typical thermal cycles imposed on a package in a cellular phone environment involve long hold times at cycle extremes. An example of this type of thermal cycle is seen when a user turns on the phone after it has been sitting in their car on a hot summer day or when the phone was left in the trunk of a car in a cold environment. These extreme conditions produce stress relaxation of the solder or creep, especially at the high-temperature end.

To characterize the solder joint reliability of the LGA package, the solder joint creep shear strain was experimentally measured via electronic speckle pattern interferometry (ESPI). The LGA specimen was placed in a thermal chamber and the temperature was varied from 25 °C to 125 °C and then held for 10 minutes. The speckle pattern at 25°C was recorded and all additional patterns were compared to this to measure the strain distribution.

In order to accurately produce an equivalent finite element model of the LGA package, the CTE and temperature dependent modulus properties of the PCB were characterized. The material properties of silicon, mold compound and solder were already known. The 2D symmetric plane strain model was developed in ANSYS™ and thermally cycled from -55 °C to 125 °C with 10 minute dwells at each peak. Each cycle lasted one hour. The model was run for three complete cycles to stabilize the hysterisis loop. The resulting sheer stress versus creep sheer strain was then plotted.

The resulting solder creep shear strain determined from both ESPI and FEA were then input into the Engelmaier lifetime prediction model. This model is then used to determine the number of cycles to failure for the LGA package. A complete description is found in Appendix B.

Reproduced with permission of the copyright owner. Further reproduction prohibited without permission.

CHAPTER 2

ELECTRONIC SPECKLE PATTERN INTERFEROMETRY

The coherency of laser light leads to the appearance of the phenomenon of speckle. This speckle pattern appears as a grainy appearance of a scattering surface when illuminated by coherent light. The speckle pattern is due to the interference that occurs between the light rays as they are scattered by different points on the surface due to the surface roughness. The resultant amplitude at any point in space is due to a set of vectors with random phase differences. The amplitude has a value which varies between zero and a maximum value. The magnitudes and phases of the individual amplitudes determine them. As the point in space is varied, the resultant intensity will have a different value. It is this random intensity variation which produces the speckle effect. The speckle effect occurs only when the surface is optically rough. This roughness must be greater than the wavelength of the illuminating beam. The size of the speckles is governed by the wavelength of light used and the aperture of the viewing system.

There are two main speckle techniques applied to surface displacement measurement; speckle photography and speckle interferometry. In speckle photography, light scattered from an object is recorded on a photographic plate. This is done before and after deformation. The two speckle patterns are produced are identical except that one is displaced relative to the other by an amount, which depends on the extent of the displacement of the object and the magnification of the imaging system. The speckle displacement can be determined by illuminating the developed plate and viewing the

Reproduced with permission of the copyright owner. Further reproduction prohibited without permission.

diffracted light. The fringes that are produced can be used to calculate the object's displacement. A hindering aspect in the process is that the plates must be developed and analyzed. Due to recent developments in digital speckle photography, the process is accelerated by eliminating the need for photographic plates. In this situation, a surface is imaged onto a CCD array and the image is sent to a computer. After the surface has been displaced another image is sent to the computer where it is digitally added to the image taken before the displacement. The resultant image can then be analyzed using digital techniques. The simple optical set-up of the technique makes it an ideal tool for non-destructive testing. Other methods such as moiré interferometry require a thin film grating to be applied to the specimen [7]. However, if the material under examination is a thin material, the applied grating can alter the properties of the material.

In electronic speckle pattern interferometry (ESPI) a speckle pattern is formed by illuminating the surface of the object to be tested, with laser light. Figure 4 shows a schematic representation of a typical ESPI setup.

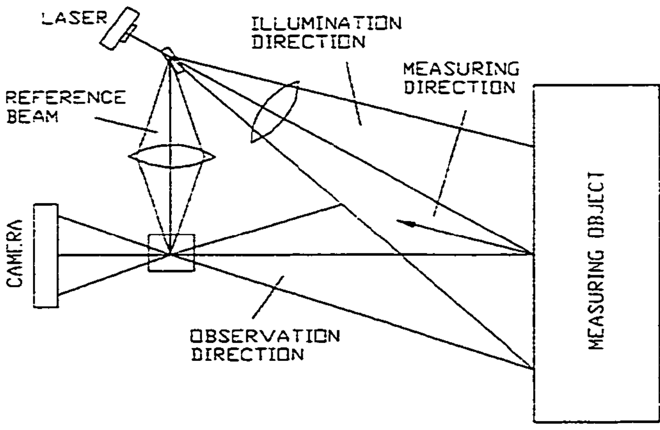

FIGURE 4. ESPI setup for strain measurements.

Reproduced with permission of the copyright owner. Further reproduction prohibited without permission.

This speckle pattern is imaged onto a CCD array where it is allowed to interfere with a reference wave as shown in Figure 5.

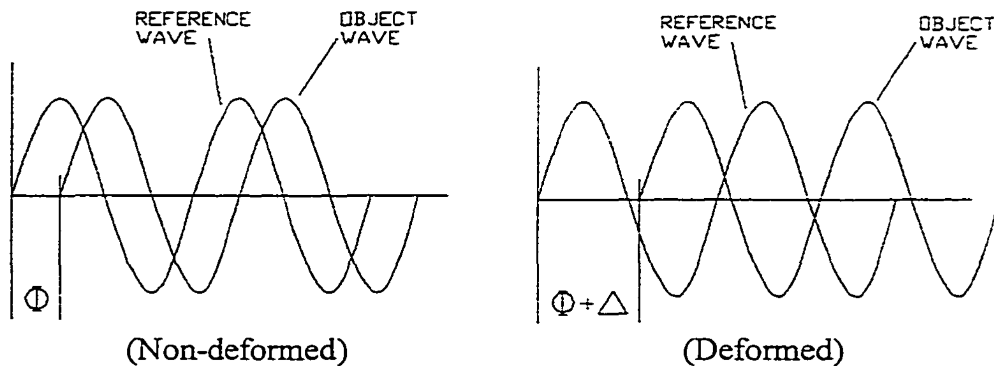

FIGURE 5. Light waves for both non-deformed and deformed patterns.

The resultant speckle pattern is then digitally captured and transferred to a computer where it is saved in memory and displayed. When the object has been deformed, or displaced, the resultant speckle pattern changes due to the change in path difference between the wavefront from the surface and the reference wave as shown in Figure 6.

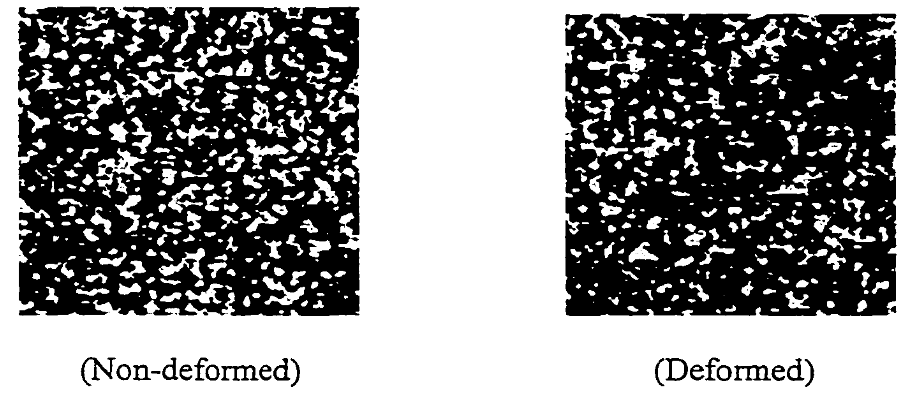

FIGURE 6. Speckle pattern of both non-deformed and deformed object.

Reproduced with permission of the copyright owner. Further reproduction prohibited without permission.

This second resultant speckle pattern is transferred to the computer and subtracted from, or added to, the previously stored pattern and the result is rectified. The resulting pattern is then displayed on the monitor as a pattern of dark and bright fringes, Figure 7. The fringes are called correlation fringes, as the fringes are produced by correlating the intensities of the resultant speckle patterns taken before and after displacement.

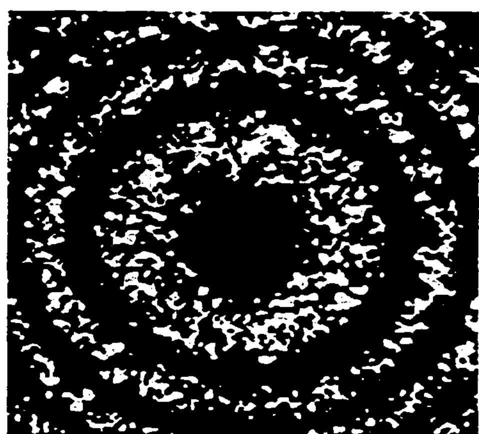

FIGURE 7. Resulting difference between original pattern and deformed pattern.

It is possible to continuously capture developing speckle patterns while a deformation is occurring and subtract them in succession from the first speckle pattern, in real-time. Using this method, it is possible to observe the real time formation and the progressive changes of the fringe pattern related to the deformation of the surface.

The similarities between ESPI and holography interferometry led to the term *TV Holography* being used to describe this technique. The result of both techniques is a fringe pattern where the fringes represent contours of equal displacement. In both techniques the fringes result from a change in phase between an object and a reference

Reproduced with permission of the copyright owner. Further reproduction prohibited without permission.

wave. The main advantage of ESPI over holographic interferometry is that it enables real-time correlation fringes to be displayed directly upon a computer monitor without any form of photographic processing or plate relocation. This comparative ease of operation allows the technique to be extended to considerably more complex problems in deformation analysis. ESPI also allows the displacement in different planes to be measured separately. Furthermore, ESPI does not require high-resolution recording media and imposes less stringent conditions on vibration isolation and ambient light. These advantages have led to an increase in the use of ESPI in a wide variety of applications. Depending on the optical configuration of the ESPI system it can be made sensitive to out-of-plane displacements, parallel to the observation direction, or in-plane displacements, perpendicular to the line of sight, or both. For an out-of-plane system, the object is viewed normal to the surface and illuminated by one beam, the object beam, at an angle near normal. The resulting speckle pattern is then imaged onto the CCD array where it interferes with a reference beam. The reference beam is aligned with the light coming from each particular part of the surface under study. The ESPI subtraction fringe patterns that are produced, represent contours of equal displacement along the viewing direction.

In an in-plane system, two beams illuminate the object at equal angles to the viewing direction, each generating its own speckle patterns. This technique only measures the displacement along a particular direction that lies normal to the line of sight of the system and in the plane of the two illumination beams. To measure strain, the displacement on the plane of the surface is measured and its variation is a function of distance in any direction can be calculated. Speckle interferometry can do this

Reproduced with permission of the copyright owner. Further reproduction prohibited without permission.

independently of any displacement taking place in the direction normal to the surface, where as holographic interferometry requires an accurate and lengthy fringe analysis. For complete in-plane displacement measurements, two such systems are needed. They measure the displacement in the same plane but in orthogonal directions. The calculated displacements can then be added together to produce the resultant in-plane displacement. By combining a dual in-plane system (sensitive to displacements in both the horizontal and vertical directions) with an out-of-plane system, it is possible to determine three-dimensional deformation of an object by recording three patterns, each with different sensitivity vectors [8].

The fringe patterns obtained by the ESPI technique represent contours of equal displacement. The spacing of the fringes is inversely proportional to the displacement and, in in-plane systems, the fringes are aligned perpendicularly to the direction of the displacement. Two consecutive dark or bright fringes represent a displacement whose exact value depends on the wavelength of the light used and the geometrical setup of the ESPI system. The value of this displacement is called the fringe sensitivity term. The measuring sensitivity can be calculated by:

$$d = \frac{N\lambda}{2\cos\left(\frac{\alpha}{2}\right)} \qquad (2\text{-}1)$$

where: d = deformation component of the object point in measuring direction

N = fringe order at the measuring point

λ = wavelength of the laser light

α = angle between illumination and the observation direction

Reproduced with permission of the copyright owner. Further reproduction prohibited without permission.

The displacement between two points can be easily calculated by simply counting the number of fringes between those points and multiplying by the fringe sensitivity term. This is known as phase-shifting. Phase-shifting is used to obtain a fringe pattern which depicts the phase change, in the range 0 and 2π, that occurred between the two speckle patterns. It is based on the introduction of a known amount of lateral shift, called the phase-step, into the interferometric pattern and the effect is a movement of intensity peaks across the pattern. The phase change is introduced either in the form of calibrated phase steps or as continuous periodic phase modulation. By analyzing the intensity patterns taken at each step the phase can be calculated. These fringe patterns can be unwrapped to produce absolute phase maps that can be subsequently analyzed to obtain accurate displacement maps.

For the strain measurements of the LGA package, a 5mm package was mounted on a PWB and cut down the centerline of the package using a diamond blade saw. Figure 8 shows a schematic of the assembly.

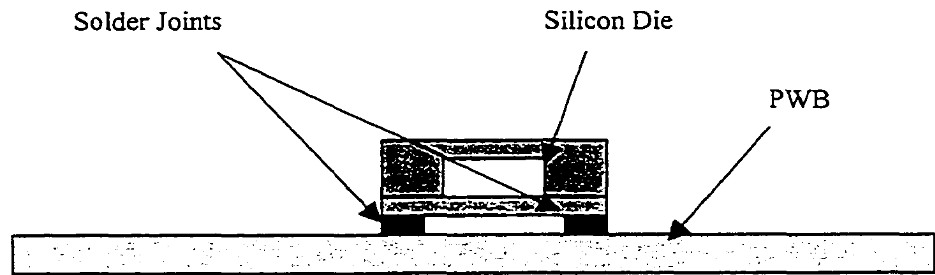

FIGURE 8. Schematic of LGA test assembly.

Reproduced with permission of the copyright owner. Further reproduction prohibited without permission.

The cross sectioned assembly was placed on a pedestal in a thermal chamber and the speckle pattern at room temperature (25^0C) was recorded. The chamber was then ramped up to 125^0C and maintained for 10 minutes. A second speckle image of the specimen was then captured and correlated to the reference image. The resulting fringe pattern representing the displacement is shown in Figure 9.

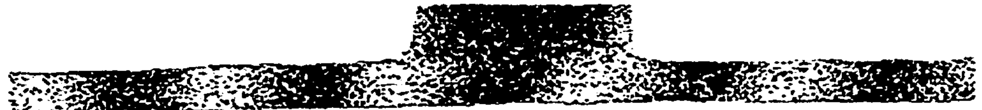

FIGURE 9. Fringe pattern from speckle pattern correlation between 125^0C and 25^0C.

With the final measured displacement determined, the resulting strain is calculated by using the centerline of the package as a reference point. The resulting strain is shown in Figure 10.

FIGURE 10. Calculated strain in the package assembly due to thermal loading.

When examining a strain pattern, the lightest shade represents little or no strain. The darkest shade represents maximum strain. As shown, the center of the package appears to be the lightest shade. This is the region were the silicon die is placed. Due to

Reproduced with permission of the copyright owner. Further reproduction prohibited without permission.

the low CTE of silicon, little strain is developed. The region were the most strain is obtained is in the solder joints. The joint on the left side of the image shows a maximum strain of 0.59%. The calculated strain value were then input into the reliability model shown in Appendix B to predict the lifetime to failure.

Reproduced with permission of the copyright owner. Further reproduction prohibited without permission.

CHAPTER 3

SUBSTRATE MATERIALS CHARACTERIZATION

To determine the material properties of the substrate composition, two different substrate material sets were used. These material sets include 200um thick bismaleimide triazine (BT) and 200um BT with 20um copper on top and bottom of the BT. Figure 11 shows the two material sets. The materials were processed this way due to the thinness of the copper foil and the inability to handle this material properly without inducing damage. This grouping of materials allows one to de-couple the properties of the copper from the BT while maintaining the material integrity.

BT RESIN – 200um

COPPER – 20um

BT RESIN – 200um

COPPER – 20um

FIGURE 11. Material set for CTE and modulus measurements.

For the coefficient of thermal expansion (CTE) measurements, one-inch square specimens were made using a water jet cutting process. The water jet cutting process allows specimens to be cut into the required shape without damaging the composite resin and helps maintain a smooth edge, reducing the effect of stress risers in the sample. A programmable hot plate was placed on its side, tilted slightly back. The hot plate

Reproduced with permission of the copyright owner. Further reproduction prohibited without permission.

needed to be placed in the orientation in order for the ESPI measurements to be possible. Five minute epoxy was used to affix a glass slide to the hot plate to be used as a platform for the substrate specimen to sit on. Epoxy was also used to hold two fused silica rods to the hot plate. The rods were used to keep the sample against the hot plate while allowing the sample to move freely underneath the rods. This freedom of movement was confirmed during measurements because the fringe pattern was continuous on both sides of the rods. If the rods were restraining the sample in any way, a step in the fringe pattern would be observed. The experimental set up is shown in Figure 12.

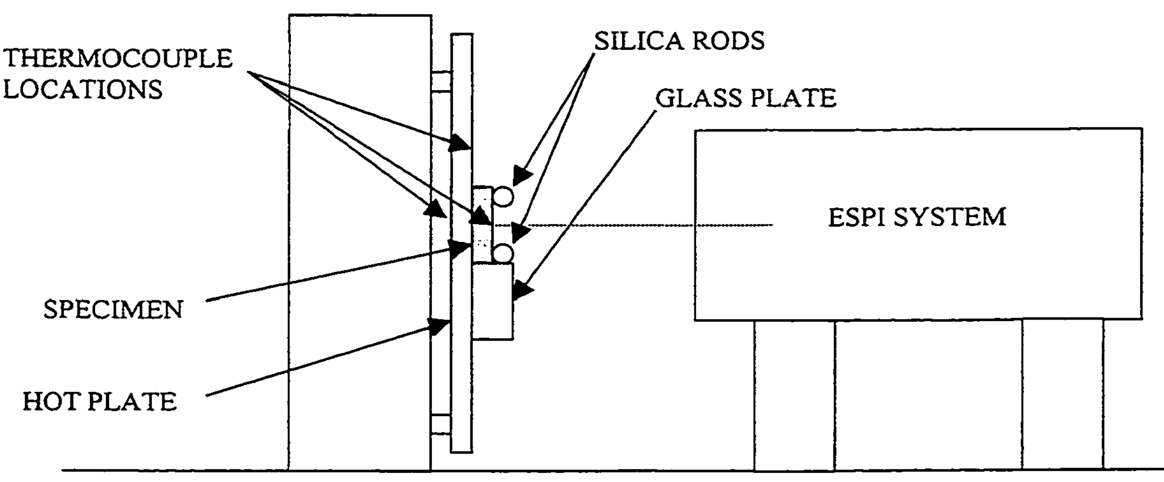

FIGURE 12. Experimental setup for CTE measurements.

When using ESPI with a hot plate, special care must be taken due to the warm air around the hot plate mixing with the cool air of the surrounding environment. The large thermal gradient that is generated between the two temperatures causes convection

Reproduced with permission of the copyright owner. Further reproduction prohibited without permission.

waves that skew the ESPI measurements. In order to resolve the problem, aluminum foil is placed around the hot plate and specimen area creating a small oven and reducing any existing thermal gradients.

A total of three thermal couples were used to monitor the temperature of the hot plate and specimen. Since these measurements were temperature dependent, it was critical that the sample temperature was known within +/-1°C. The first thermocouple was used to control the temperature of the oven and was placed on the bottom side of the hot plate directly below the sample. The second thermal couple was placed adjacent to the specimen on the hot plate using epoxy. The third was rolled up like a spring and placed on top of the specimen keeping constant pressure without the use of epoxy. This allowed for temperature measurements while not constraining the sample.

During experiments, the temperature was ramped at 1.5°C/min up to 150 °C maximum. This slow rate of heating ensured the temperature of the sample remained near the temperature of the hot plate and that no thermal gradients existed between the top and bottom of the sample. If thermal gradients did exist between the top and bottom of the sample, the specimen would bend away from the hot plate. This would both skew the temperature of the specimen as well as the displacement measurement. Data was collected in approximately 10°C increments. The recorded displacements from ESPI were first converted into strain measurements for the samples and plotted as a function of temperature. A typical graph of the strain versus temperature is shown in Figure 13. As shown, the material behaves fairly linear over the entire range for this analysis.

Reproduced with permission of the copyright owner. Further reproduction prohibited without permission.

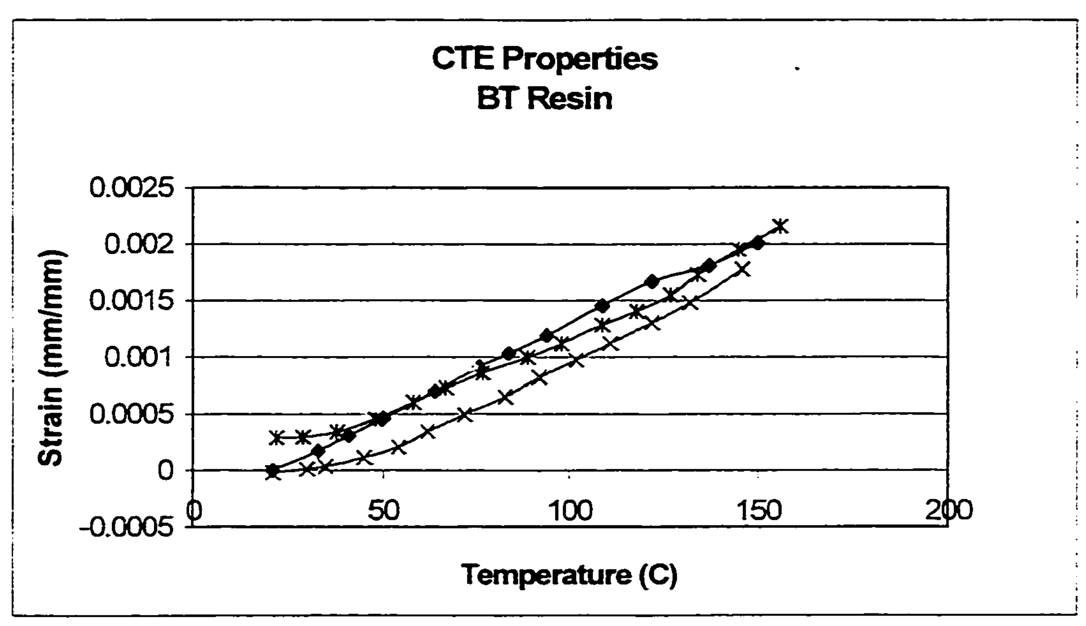

FIGURE 13. Graph of strain versus temperature result for BT.

A total of three samples per material set were tested. Each individual sample specimen measurement was repeated once to verify results. With the strain values versus temperature known, the slope was determined. This slope is the resulting temperature dependent CTE value, as shown in Table 2. All of the raw data and final calculated CTE measurements can be found in Appendix C.

TABLE 2. Calculated Temperature Dependent CTE Value of Sample Number One

Sample #1	Temp (C)	Strain (%)	CTE (slope)
	21	0.00E+00	-
	33	1.71E-04	14.3
	41	3.12E-04	17.5
	50	4.63E-04	16.8
	64	7.00E-04	16.9
	76	9.12E-04	17.7
	84	1.03E-03	14.7
	94	1.19E-03	16.0
	109	1.46E-03	17.7
	122	1.67E-03	16.4
	137	1.81E-03	15.8
	150	2.01E-03	15.3

Reproduced with permission of the copyright owner. Further reproduction prohibited without permission.

For the temperature dependent modulus measurements of the BT and copper materials, specimens were cut using the water jet process similar to the CTE specimens above. The size and shape of the specimens followed similar to ASTM standards for modulus determination but slightly shorter in length so they could fit in the thermal chamber. The dimension details of the samples are shown in Figure 14.

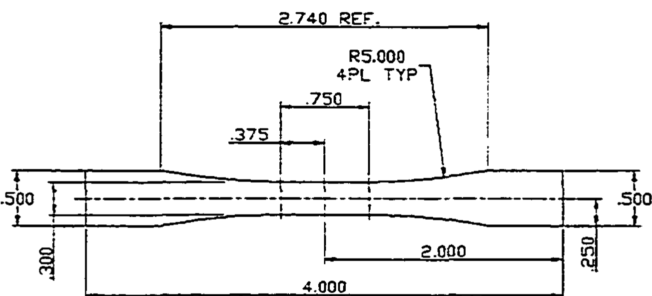

FIGURE 14. Dog bone specimen used to determine modulus (dimensions in inches).

With the specimens generated, the modulus values of the BT and copper were determined using an Instron™ 5500 series Microforce Tester. This electromechanical driven tensile tester uses a 200 lb load cell attached to its base. Two large steel pillars come up from the base to support the servo driven loading arm and the numerically controlled thermal chamber. The chamber is capable of up to 220°C and the heating elements and blower are located in another chamber placed on the floor, below the system. Three-inch diameter inlet and exhaust tubes connect the chamber to the heating unit. This method allows the application of temperature dependency measurements without causing distortion due to vibration of the heating unit. The steel wedge grips, rated at 5,000 lb each, were used to hold the specimen. They were located inside the chamber with the specimen. The strain measurements were recorded using a strain

Reproduced with permission of the copyright owner. Further reproduction prohibited without permission.

extensometer attached to the gauge length region of the specimen. The recorded values were automatically loaded into the Instron™ software and plotted versus the measured load. The experimental setup is shown in Figure 15.

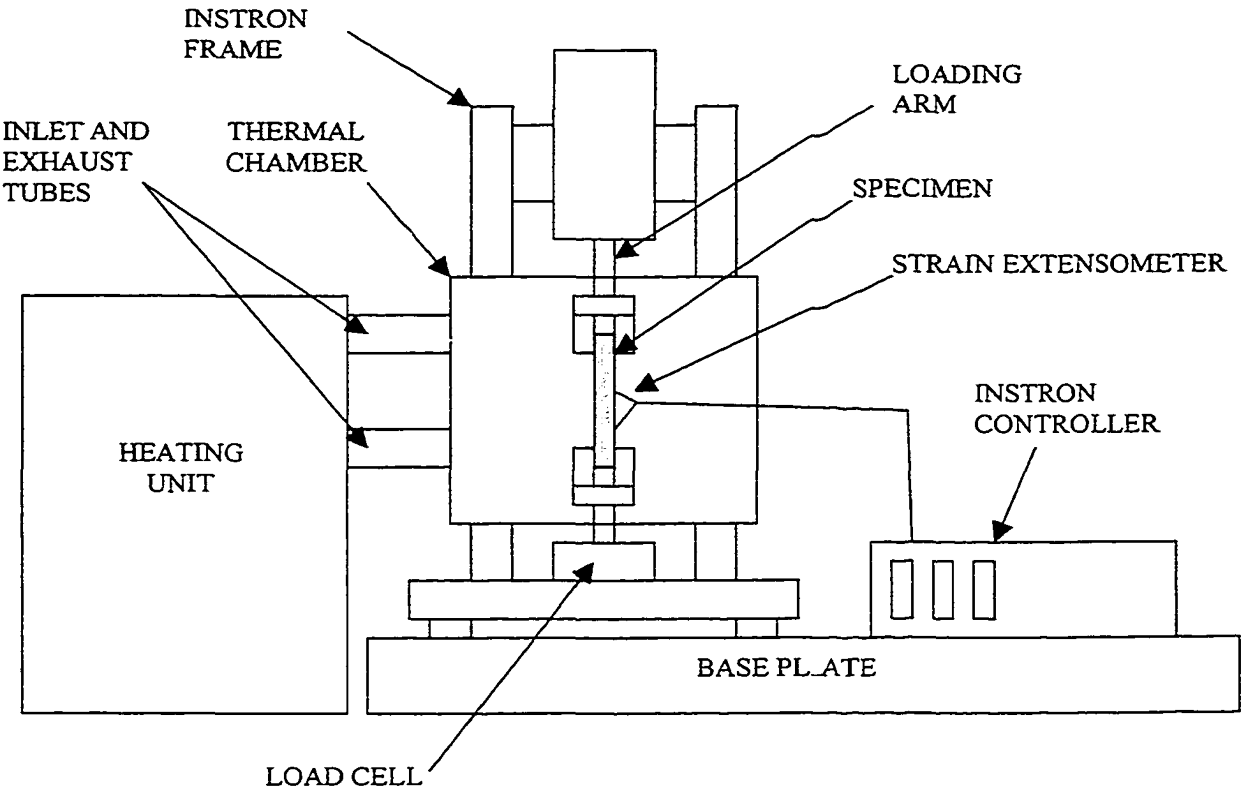

FIGURE 15. Experimental setup for modulus testing.

To determine the modulus of the BT and copper, three specimens were tested at each of three temperatures: 25°C, 100°C, and 150°C. For each specimen measurement, the sample was placed in the preheated chamber and allowed to soak for 10 minutes. This required soaking time to bring the specimen up to temperature was confirmed using a thermal couple during the experimental setup. For the actual testing, the thermal couple was removed. The modulus properties of the materials below 25°C were

Reproduced with permission of the copyright owner. Further reproduction prohibited without permission.

assumed to behave identical to the properties at 25°C. By measuring three samples at each temperature, repeatability of the testing was confirmed. The graph of the stress-strain curve of BT resin at the measured temperatures is shown in Figure 16. Both the experimental data and bilinear fit model are shown.

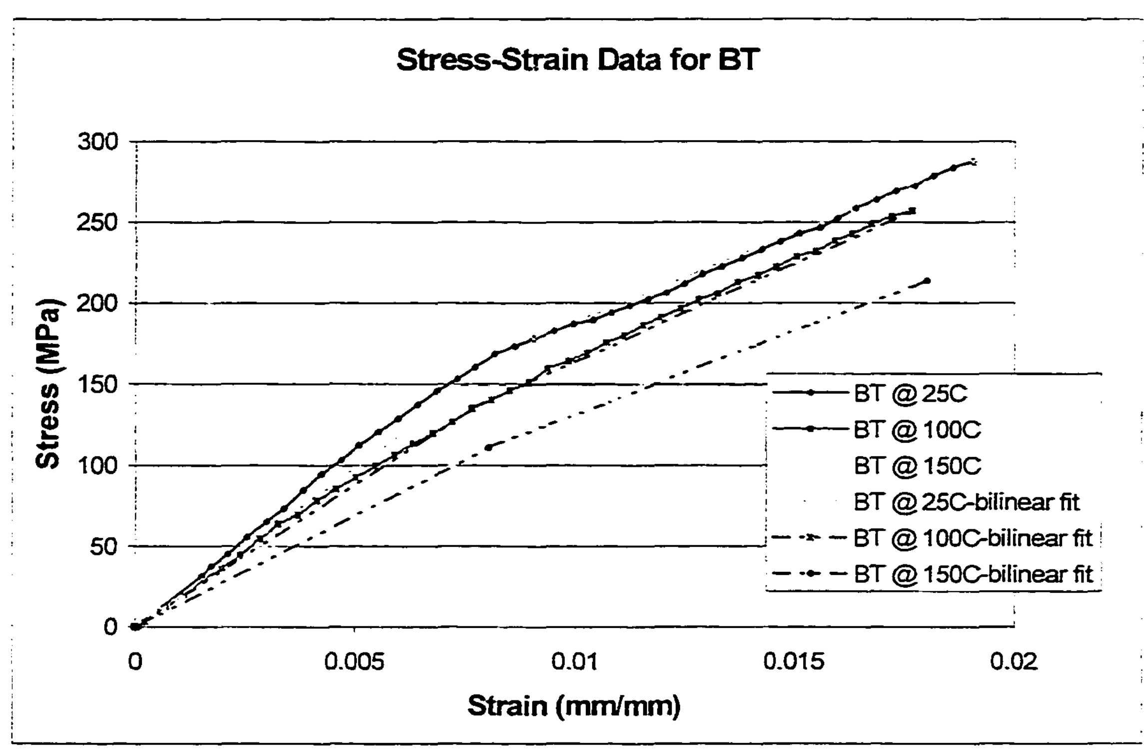

FIGURE 16. Experimental data and bilinear model of BT resin at the three temperatures.

With the CTE and temperature dependent modulus obtained for the BT resin and the copper foil, ANSYS™ input files were generated representing the two materials. The properties of all other materials involved in this electronic package assembly were obtained from previous experiments and industry standard databases.

Reproduced with permission of the copyright owner. Further reproduction prohibited without permission.

CHAPTER 4

EQUIVALENT FINITE ELEMENT MODEL

With the experimental creep shear strain data obtained via ESPI and the CTE and temperature dependent modulus determined, a two-dimensional plane strain half-symmetric model was generated using ANSYS™ finite element analysis. Typically, three dimensional quarter models are used to determine thermal strains due to CTE mismatches. However, when finite element models involving time dependency (creep shear strain) are used, the number of degrees of freedom must be kept to a reasonable size due to computational constraints. In this case, the model was kept under 50,000.

For a simple three-dimensional linear stress-strain relationship, the stress is related to strain by:

$$\{\sigma\} = [D]\{\varepsilon^{el}\} \qquad (4\text{-}1)$$

where: $\{\sigma\}$ = stress vector = $[\sigma_x\, \sigma_y\, \sigma_z\, \sigma_{xy}\, \sigma_x\, \sigma_{yz}\, \sigma_{xz}]^T$

$[D]$ = elasticity matrix

$\{\varepsilon^{el}\}$ = $\{\varepsilon\}$ - $\{\varepsilon^{th}\}$ = output quantity

$\{\varepsilon\}$ = total strain vector = $[\varepsilon_x\, \varepsilon_y\, \varepsilon_z\, \varepsilon_{xy}\, \varepsilon_x\, \varepsilon_{yz}\, \varepsilon_{xz}]^T$

$\{\varepsilon^{th}\}$ = thermal strain vector

Equation (4-1) may be inverted to:

$$\{\varepsilon\} = \{\varepsilon^{th}\} + [D]^{-1}\{\sigma\} \qquad (4\text{-}2)$$

The thermal strain vector is shown as:

Reproduced with permission of the copyright owner. Further reproduction prohibited without permission.

$$\{\varepsilon^{th}\} = \Delta T\,[\alpha_x\,\alpha_y\,\alpha_z\,0\;0\;0\,]^T \qquad (4\text{-}3)$$

where: α_x = thermal coefficient of expansion in the x direction

$\Delta T = T - T_{REF}$

T = current temperature at the point in question

T_{REF} = strain-free reference temperature

$$[D]^{-1} = \begin{bmatrix} \frac{1}{E_x} & \frac{-v_{xy}}{E_y} & \frac{-v_{xz}}{E_z} & 0 & 0 & 0 \\ \frac{-v_{yx}}{E_x} & \frac{1}{E_y} & \frac{-v_{yz}}{E_z} & 0 & 0 & 0 \\ \frac{-v_{zx}}{E_x} & \frac{-v_{zy}}{E_y} & \frac{1}{E_z} & 0 & 0 & 0 \\ 0 & 0 & 0 & \frac{1}{G_{xy}} & 0 & 0 \\ 0 & 0 & 0 & 0 & \frac{1}{G_{yz}} & 0 \\ 0 & 0 & 0 & 0 & 0 & \frac{1}{G_{xz}} \end{bmatrix} \qquad (4\text{-}4)$$

where: E_x = Young's modulus in the x direction

v_{xy} = minor Poisson's ratio

G_{xy} = shear modulus in the xy plane

In the case of temperature dependent coefficient of thermal expansion properties, like the substrate material, CTE is shown as:

$$\varepsilon^{th} = \int_{T_{REF}}^{T} \alpha_{inst}(T)\,dT \qquad (4\text{-}5)$$

where: $\alpha_{inst}(T)$ = instantaneous coefficient of thermal expansion

In ANSYS™ however, the instantaneous CTE must be converted to the mean or effective value of α as:

Reproduced with permission of the copyright owner. Further reproduction prohibited without permission.

$$\varepsilon^{th} = \overline{\alpha}(T)(T - T_{REF}) \qquad (4\text{-}6)$$

where: $$\overline{\alpha}(T) = \frac{\int_{T_{REF}}^{T} \alpha_{inst}(T)dT}{T - T_{REF}} = \text{mean value of CTE}$$

If the mean value of CTE is not used in the analysis, the result will be calculated incorrectly. The T_{REF} is not only the initial temperature at which all thermal strains are calculated, it is the temperature at which zero strains in the model exist. The distinction between instantaneous CTE and effective CTE is shown in Figure 17. In the case of this analysis, the temperature at which zero thermal strain occurs is assumed to be 183^0C. The temperature at which 63/37 SnPb solder reflows.

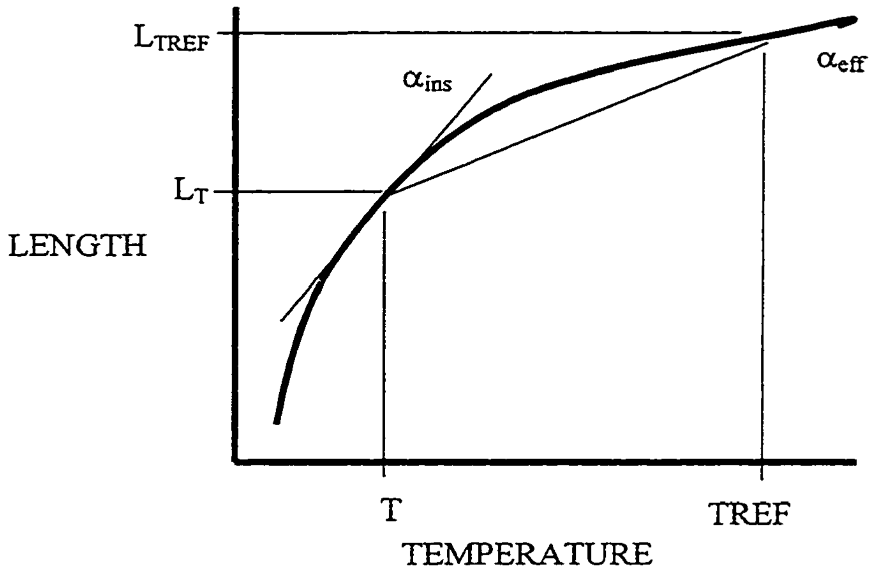

FIGURE 17. Difference of instantaneous CTE and effective CTE.

Most common engineering materials exhibit a linear stress-strain relationship up to a stress level known as the proportional limit. Beyond this limit, the stress-strain relationship will become nonlinear, but will not necessarily become inelastic. Plastic

Reproduced with permission of the copyright owner. Further reproduction prohibited without permission.

behavior, characterized by nonrecoverable strain, begins when stresses exceed the material's yield point.

From the substrate material characterization described previously, the resulting temperature dependent modulus of the BT and copper were input into the ANSYS™ finite element model. Two approaches were used to represent the BT and copper and the results were compared versus the required simulation time. It was first thought that the materials would behave in the typical elastic-plastic fashion and an exponential fit [9] could be used. Another approach considered was to use a reduced modulus based on the elastic and tangential modulus [10]. However, the tangential modulus of the plasticity behaved similarly to the elastic modulus. Therefore, it was determined to use a bilinear fit model to represent the modulus properties of each material. Figure 18 shows how the bilinear fit modulus is generated from the elastic and tangential modulus.

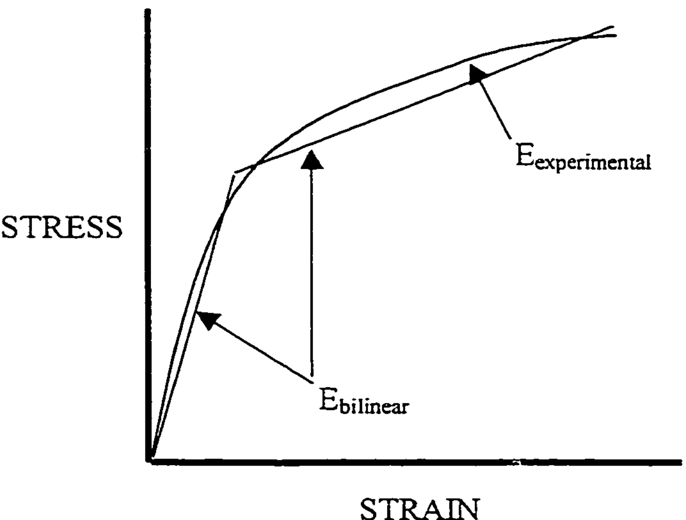

FIGURE 18. Method for determining the bilinear fit modulus from experimental data.

Reproduced with permission of the copyright owner. Further reproduction prohibited without permission.

The second method used for the modulus accounts for multilinear isotropic hardening. This allows the user to describe the stress-strain relationship of the materials at several temperatures including the work hardening of the material. An example of multilinear isotropic material properties is shown in Figure 19. During an analysis, at any one particular temperature between two temperature curves, ANSYS™ assumes a linear interpolation to determine the exact material properties at that point. For this second part of the analysis, the measured data and 25^0C, 100^0C, and 150^0C was used.

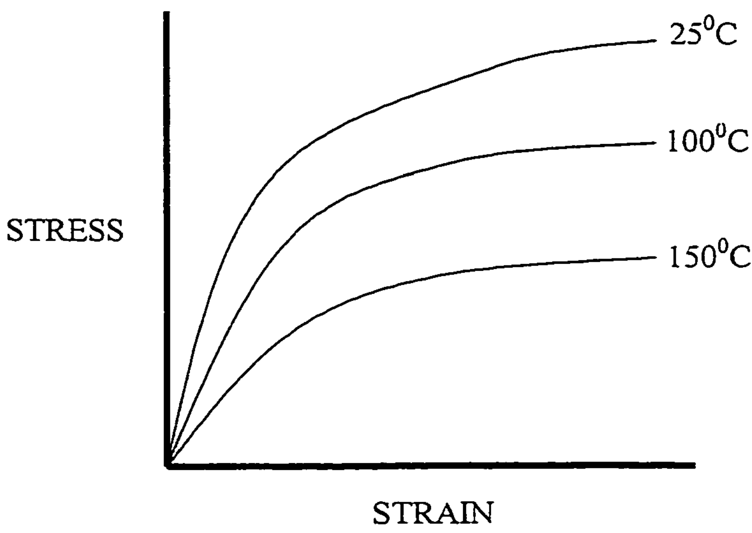

FIGURE 19. Format for a multilinear isotropic hardening material property.

When the strains in a material, such as solder, exceed more than a few percent, the changing geometry due to this deformation can no longer be neglected. Analyses, which include this effect, are referred to as large strain analyses. The large strain computations can be addressed by defining the mathematical relationship between motion and deformation. When a thermal load is applied to the body, the body moves

Reproduced with permission of the copyright owner. Further reproduction prohibited without permission.

from one position to another. The motion can be defined by studying a position vector in the deformed and undeformed configuration. Consider the position vectors in Figure 20. In the deformed and underformed state, {x} and {X} respectively, then the displacement vector is shown as:

$$\{u\} = \{x\} - \{X\} \tag{4-7}$$

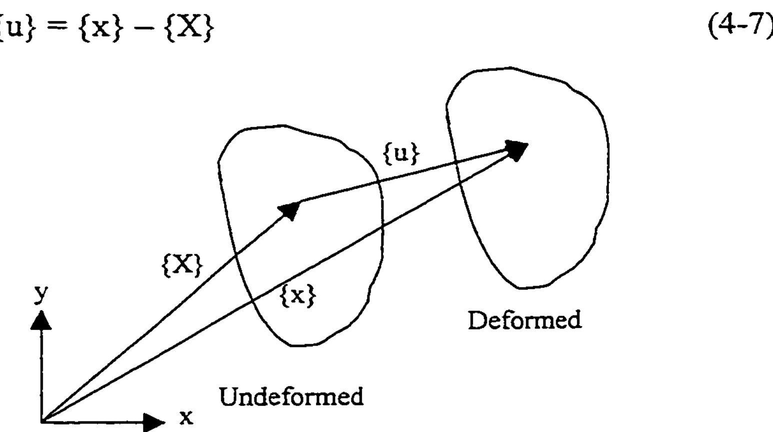

FIGURE 20. Position vectors and motion of a deforming body.

The deformation gradient is defined as:

$$[F] = \frac{\partial\{x\}}{\partial\{X\}} \tag{4-8}$$

which can be written in terms of the displacement as:

$$[F] = [I] + \frac{\partial\{u\}}{\partial\{X\}} \tag{4-9}$$

where: [I] = identity matrix

The deformation gradient can be separated into a rotation and a shape change using the right polar decomposition theorem:

$$[F] = [R]\,[U] \tag{4-10}$$

Reproduced with permission of the copyright owner. Further reproduction prohibited without permission.

where: [R] = rotation matrix ($[R]^T [R] = [I]$)

[U] = shape change matrix

With the shape change matrix known, a logarithmic strain measure is defined as:

$$[\varepsilon] = \ln [U] \quad (4\text{-}11)$$

where ε is in tensor matrix form. In this case [U] is a second order tensor matrix and ε is determined through the spectral decomposition of [U]:

$$[\varepsilon] = \sum_{i=1}^{3} \ln(\lambda_i)\{e_i\}\{e_i\}^T \quad (4\text{-}12)$$

where: λi = eigenvalues of [U] (principal shape change)

$\{e_i\}$ = eigenvectors of [U] (principal directions)

The polar decomposition theorem extracts a rotation [R] that represents the average rotation of the material at a point. Material lines initially orthogonal are not typically orthogonal after deformation due to shearing [11].

Creep is a rate dependent material nonlinearity is which the material continues to deform under a constant load [12]. If a displacement is imposed, the reaction force and stresses will diminish over time due to stress relaxation. The three stages of creep are shown in Figure 21. In typical applications the first two stages are generally modeled. However, the tertiary stage is not commonly considered due to the impending failure.

Reproduced with permission of the copyright owner. Further reproduction prohibited without permission.

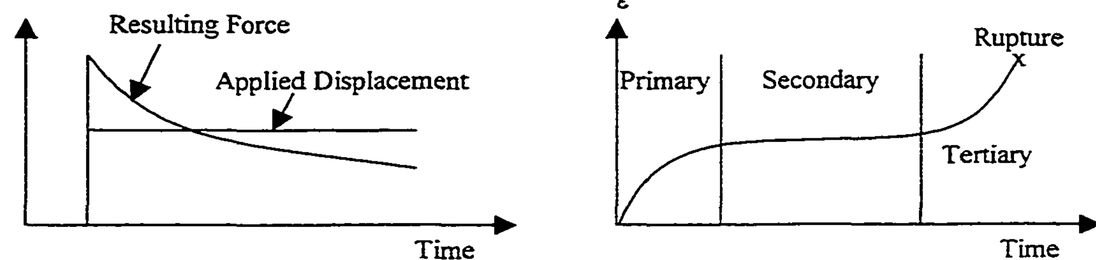

FIGURE 21. Stress relaxation and creep phenomenon.

Creep becomes extremely important at high temperatures relative to the melting temperature of a material. In the case of 63/37 SnPb solder, the melting point is 183^{0}C or 456 Kelvin. The maximum temperature for thermal cycling is 125^{0}C or 398 Kelvin, which is 87% of the melting temperature. Extensive experimental analysis has been performed to characterize the creep strain rate (dγ/dt) of 63/37 SnPb solder. For this analysis, the hyperbolic sine law is used to model the creep strain rate and as shown in its general form as:

$$\frac{\partial \gamma}{\partial t} = C_1[\sinh(C_2\sigma)]^{C_3} e^{\frac{C_4}{T}} \qquad (4\text{-}13)$$

where: C_1,C_2, and C_3 = material constants

σ = equivalent stress

C_4 = ΔH/R

ΔH = activation energy of 63/37 SnPb solder (J/mol)

R = universal gas constant (J/mol – K)

T = absolute temperature (K)

Filling in for constants C1, C2, C3, and C4 to represent the 63/37 SnPb solder, equation (4-11) becomes:

Reproduced with permission of the copyright owner. Further reproduction prohibited without permission.

$$\frac{\partial \gamma}{\partial t} = 1.30x10^{6}[\sinh(0.102\sigma)]^{2.4} e^{\frac{9116.78}{T}} \quad (4\text{-}14)$$

With the material properties of the package assembly defined, a two-dimensional, half symmetry model was generated using the ANSYS™ Parametric Design Language (APDL™). Variables describing the geometry of the packaging assembly were entered in as a text file and loaded into ANSYS™. The complete APDL™ commands required to generate the model, material properties, and loading is shown in Appendix C.

The Plane183 structural element was chosen for this plane strain analysis because it is a higher order eight-noded element with quadratic displacement behavior. It is well suited for large strain applications because it uses a consistent tangent stiffness. Each of the eight nodes has two degrees of freedom: translation in X and Y directions and has plasticity, creep, stress stiffening, large deflection, and large strain. Particularly for low cycle creep calculations, the Plane183 element provides the most robust solution of any two-dimensional plane element. A pictorial view of the element is shown in Figure 22.

Reproduced with permission of the copyright owner. Further reproduction prohibited without permission.

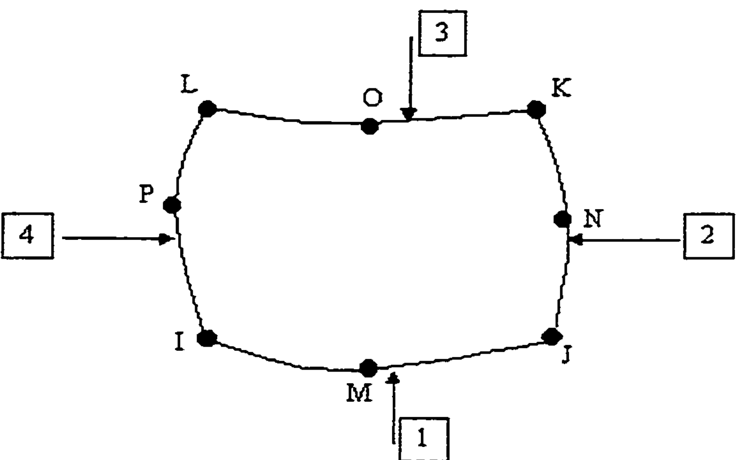

FIGURE 22. Plane183 two-dimensional eight node structural element.

Using the APDL™ command language, a mapped mesh was applied to the areas of the model to produce a extremely fine mesh around the solder joint region while leaving other, less critical areas of the model with a coarser mesh. Mesh sensitivity analysis was performed to ensure that a fine enough mesh was applied. The resulting finite element model is shown in Figure 23.

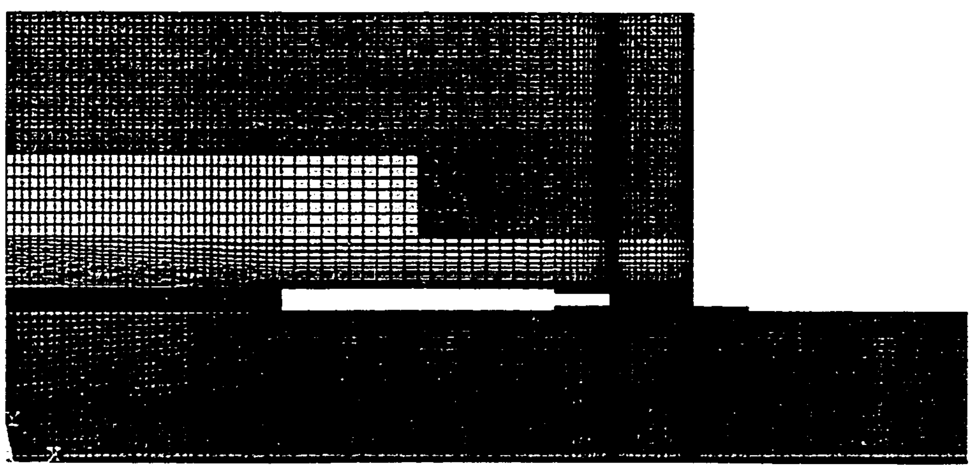

FIGURE 23. Final half symmetry mesh pattern of 5mm LGA package.

Reproduced with permission of the copyright owner. Further reproduction prohibited without permission.

To apply the thermal loading to the model, the temperature versus time, thermal cycle, was defined and a loop was generated to repeat the –55°C to 125°C one hour cycle three times. The significance of three cycles is due to the number of cycles required for the hysteresis loop to stabilize. The minimum and maximum time step increment was defined to assist the solutions convergence and the Newton-Raphson iterative process of solving the nonlinear equations was selected. The resulting creep strain versus time and hysteresis loop from the model with experimentally measured material properties is shown in Figures 24 and 25.

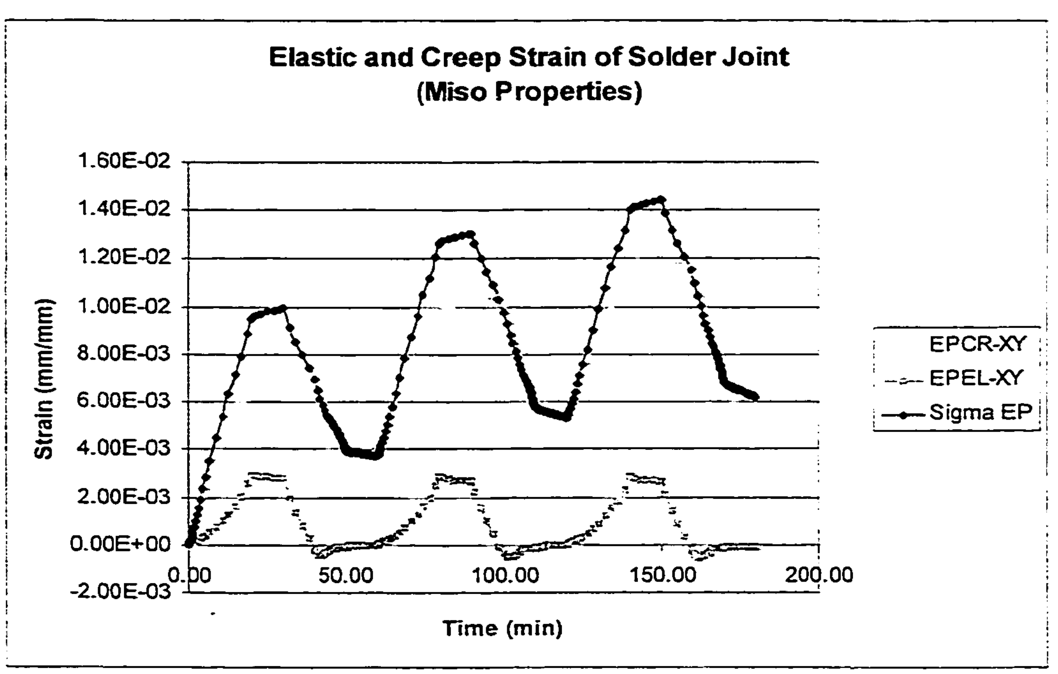

FIGURE 24. Elastic, creep, and total shear strain plotted versus time, multilinear.

Reproduced with permission of the copyright owner. Further reproduction prohibited without permission.

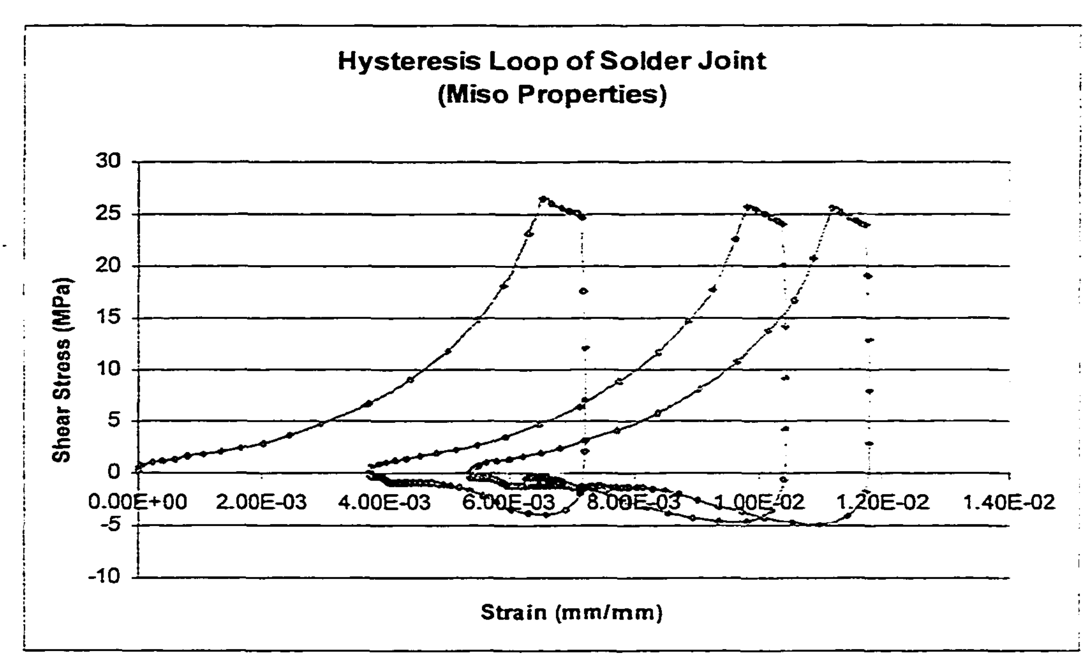

FIGURE 25. Hysteresis loop of solder joint, multilinear.

The bilinear material properties of the BT and copper when then applied to the same model and the analysis was performed Figures 26 and 27 show the shear strain versus time and the resulting hysteresis loop.

Reproduced with permission of the copyright owner. Further reproduction prohibited without permission.

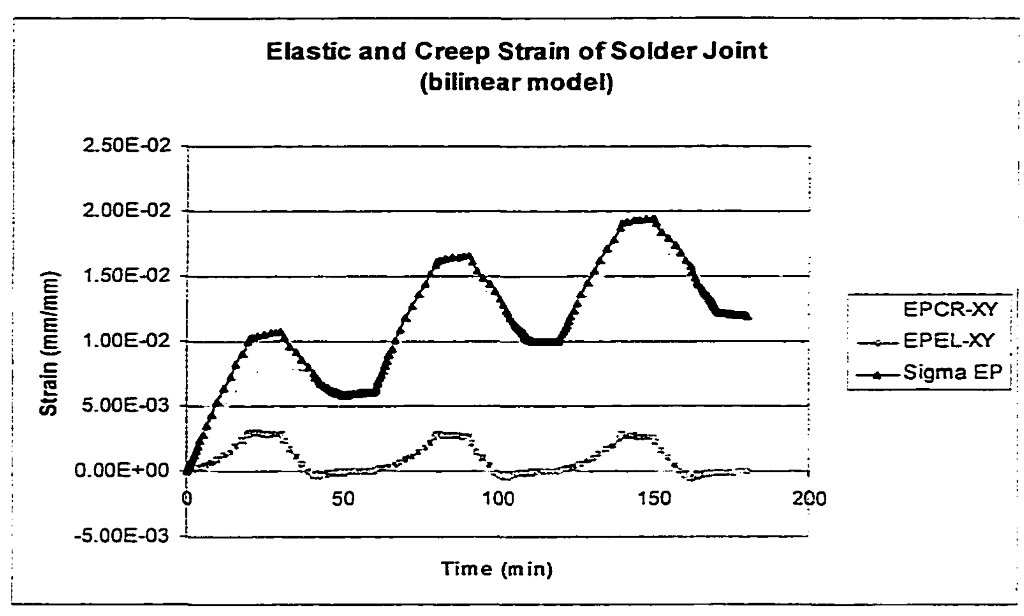

FIGURE 26. Elastic, creep, and total shear strain plotted versus time, bilinear.

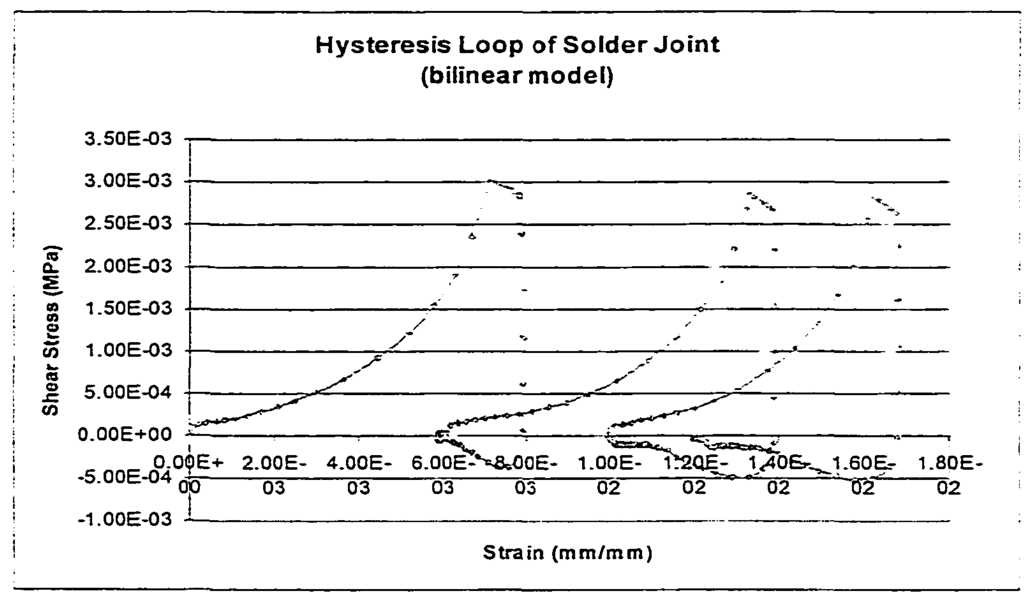

FIGURE 27. Hysteresis loop of solder joint, bilinear.

Reproduced with permission of the copyright owner. Further reproduction prohibited without permission.

CHAPTER 5

CONCLUSION

As described herein, a new methodology has been applied to determine the solder joint strain in the 2nd level interconnect of a cross sectioned 5mm land grid array electronic package. By using Electronic Speckle Pattern Interferometry, one eliminates the requirement of applying a thin film grating to the surface of the test specimen as required with Moiré Interferometry, which has been the standard method for whole field measurements in the electronic packaging. When applying the fringe grating, the results of interest may become skewed because Moiré is actually measuring the thin film grating instead of the specimen. Moreover, with ESPI, the sample preparation becomes much easier because the whole field displacement measurements do not have to initiate at the thin film grating cure temperature as required with Moiré. This allows one to apply the exact thermal loading constraints on the specimen, as they would be applied in the real world application.

In addition to the package level solder joint strain measurements, ESPI was also used to determine the CTE properties of BT and copper materials found in the LGA substrate. Sample specimens were placed on a digitally controlled hot plate and the resulting strains at temperature were recorded. These strains were then used to determine the CTE values of the two materials. The CTE of both materials behaved fairly constant throughout the desired temperature range, 25^0C to 125^0C. The BT was found to have a CTE of 16.2ppm and the CTE of copper was determined to be 21.2ppm.

Reproduced with permission of the copyright owner. Further reproduction prohibited without permission.

Specimens of the BT and copper materials were cut from a 12" by 12" panel using a waterjet cutting process. Each specimen was individually loaded into an Instron™ 5548 Micro Force Tester to determine the temperature dependent modulus. Measurements were performed at 25^0C, 100^0 C, and 150^0 C. From the measured data, a multilinear isotropic model representing the exact data and a bilinear model representing the elastic and plastic modulus were generated to represent each material and at each of the three temperatures. As expected, when the temperature of each material increased, both the elastic and plastic modulus decreased. At 25^0C, the elastic modulus of the BT and copper were determined to be 19.8Gpa and 125Gpa, respectively.

A two-dimensional, plane strain finite element model was developed and the measured material properties were loaded into the model using the exact experimental data and a bilinear fit approximation. A hyperbolic sine creep strain rate equation was used to represent the solder alloy. Appropriate boundary conditions were applied and three equivalent temperature cycles from -55^0C to 125^0C with 10 minute dwells, were loaded. Using a custom algorithm developed for this model, the solder joint elements exhibiting the highest shear strain were selected and the creep shear strain over the selected elements was averaged. This method eliminated any singularity effects caused by finite element modeling. The convergence of the stress-strain hysteresis loop for each model was confirmed and the difference between the highest and lowest creep shear strain per cycle was determined. This difference represents the total non-recoverable creep shear strain per cycle.

Reproduced with permission of the copyright owner. Further reproduction prohibited without permission.

The resulting strain from each of the three methods, both measured and numerically solved, was plugged into the Engelmaier reliability prediction model, shown in Appendix B. The resulting strain and cycles to failure are shown in Table 3.

TABLE 3. Experimental and Numerical Reliability Results

Method	ESPI Method (Experimental)	FEM - Bilinear Substrate	FEM - Multilinear Substrate
Plastic Shear Strain, $\Delta\gamma$ (%)	0.59	0.682	0.642
Number of Cycles to Failure, N_F	7485	5880	6503

As shown in Table 3, the experimental technique showed the lowest amount of strain in the solder joint. Both finite element models calculated higher strain in the solder joint with the bilinear model showing the largest amount of strain. The difference in results between the two models is believed to be due to interpolation of the bilinear material properties. However, the two results are within 6% of one another. As expected, the multilinear material properties model predicted more accurate results when compared to the ESPI results, within 9%. The bilinear model predicted results within 16%. However, due to the more linear behavior of the bilinear material properties, only 4 hours of computation time were required versus 9 hours using the multilinear properties. In all cases, the failure of the solder joint was determined to be Mode II.

While the author performed the temperature dependent modulus characterization and development of the numerical models, assistance was obtained using outside

Reproduced with permission of the copyright owner. Further reproduction prohibited without permission.

resources to measure the coefficient of thermal expansion of the BT and copper materials as well as the shear strain measurements of the package assembly.

Reproduced with permission of the copyright owner. Further reproduction prohibited without permission.

APPENDICES

Reproduced with permission of the copyright owner. Further reproduction prohibited without permission.

APPENDIX A

EXPERIMENTAL MATERIAL PROPERTIES

Reproduced with permission of the copyright owner. Further reproduction prohibited without permission.

CTE measurements were performed on BT and copper materials as described in chapter three using speckle interferometry. The measured properties for BT is shown in Tables 4-6.

TABLE 4. Measured CTE Values of BT, Sample #1.

Temp (C)	Strain (%)	CTE (slope)
21	0.00E+00	
33	1.71E-04	14.3
41	3.12E-04	17.5
50	4.63E-04	16.8
64	7.00E-04	16.9
76	9.12E-04	17.7
84	1.03E-03	14.7
94	1.19E-03	16.0
109	1.46E-03	17.7
122	1.67E-03	16.4
137	1.81E-03	15.8
150	2.01E-03	15.3
	Average =>	16.3

TABLE 5. Measured CTE Values of BT, Sample #2.

Temp (C)	Strain (%)	CTE (slope)
21	-1.92E-05	15.6
30	1.32E-05	16.4
35	3.58E-05	15.7
45	1.13E-04	15.9
54	2.05E-04	16.2
62	3.44E-04	17.1
72	4.93E-04	15.7
83	6.51E-04	15.2
92	8.23E-04	18.2
102	9.73E-04	15.7
111	1.12E-03	16.5
122	1.30E-03	16.7
132	1.48E-03	17.7
146	1.78E-03	18.3
160	2.02E-03	17.7
	Average =>	16.6

Reproduced with permission of the copyright owner. Further reproduction prohibited without permission.

TABLE 6. Measured CTE Values of BT, Sample #3.

Temp (C)	Strain (%)	CTE (slope)
22	2.91E-04	13.6
29	2.95E-04	15.3
38	3.42E-04	15.6
48	4.50E-04	15.6
58	6.04E-04	15.4
67	7.29E-04	15.2
77	8.63E-04	14.8
89	9.96E-04	15.2
98	1.12E-03	15.8
109	1.28E-03	15.1
118	1.40E-03	14.9
127	1.55E-03	16.1
134	1.73E-03	18.4
145	1.95E-03	17.8
156	2.16E-03	18.8
	Average =>	15.8

As shown, all three sample specimens behaved fairly linearly within the temperature range examined. Figure 28 shows all collected data. At the low temperature of 25^0C the lowest CTE measurement was recorded at 13.6 ppm. At temperatures above 100^0C, the maximum CTE was found to be 18.8 ppm. Based on this information, an average CTE value was calculated. This value was found to be 16.2 ppm.

Reproduced with permission of the copyright owner. Further reproduction prohibited without permission.

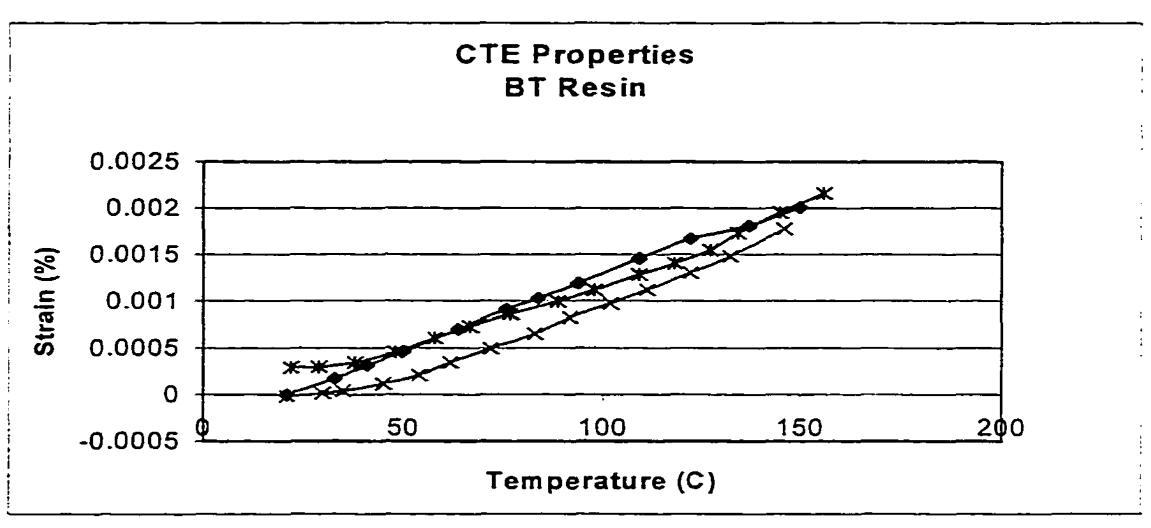

FIGURE 28. Measured strain values versus temperature for BT resin.

The CTE measurements for the copper material are shown in Tables 7-9. The procedure used to determine the properties follows the method used for the BT material.

TABLE 7. Measured CTE Values of Copper, Sample #1.

Temp (C)	Strain (%)	CTE (slope)
22.5	-2.41E-04	
28	-9.75E-05	21.8
36.2	8.83E-05	22.7
46.5	2.88E-04	20.4
56.7	4.93E-04	20.1
67.3	7.19E-04	21.3
76.1	9.18E-04	22.7
85	1.12E-03	22.4
100.8	1.48E-03	23.1
114	1.78E-03	22.7
127.5	2.08E-03	22.3
136	2.35E-03	21.4
150.8	2.66E-03	20.9
	Average =>	21.8

Reproduced with permission of the copyright owner. Further reproduction prohibited without permission.

TABLE 8. Measured CTE Values of Copper, Sample #2.

Temp (C)	Strain (%)	CTE (slope)
21	-2.41E-04	
31	-5.77E-05	18.4
41	1.53E-04	21.0
51	3.66E-04	21.4
61	5.78E-04	21.2
69.6	7.66E-04	21.8
79.6	9.59E-04	19.3
85.1	1.06E-03	19.3
93.8	1.23E-03	19.1
100.2	1.35E-03	19.1
110	1.56E-03	20.8
118.6	1.78E-03	23.1
125.2	1.95E-03	22.4
132.7	2.12E-03	22.7
141.1	2.33E-03	23.7
152.2	2.67E-03	22.3
	Average =>	21.0

TABLE 9. Measured CTE Values of Copper, Sample #3.

Temp (C)	Strain (%)	CTE (slope)
21	0.00E+00	
32	1.89E-04	21.8
42	3.84E-04	20.2
54	6.08E-04	19.4
65	8.24E-04	19.9
77	1.04E-03	20.8
87	1.25E-03	20.6
97	1.41E-03	19.9
106	1.59E-03	21.8
116	1.77E-03	21.6
125	1.94E-03	20.4
135	2.13E-03	21.1
144	2.31E-03	21.3
150	2.41E-03	22.4
	Average =>	20.9

Reproduced with permission of the copyright owner. Further reproduction prohibited without permission.

Similar to the BT resin material, the copper material was found to act fairly linear as well. A minimum value of 18.4 ppm was measured at low temperature and a maximum of 23.7 ppm was found near the high temperature end. The average of all three sample sets was found to be 21.2 ppm. The graph representing the recorded data is found in Figure 29.

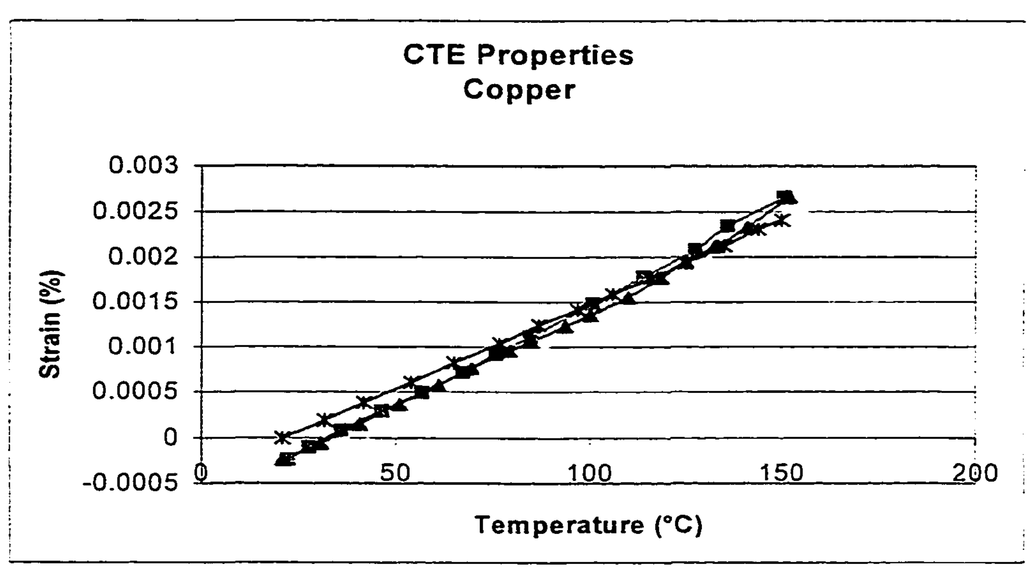

FIGURE 29. Measured strain value versus temperature for copper material.

The modulus measurements were performed using an Instron™ 5548 Micro Force tester. The experimental setup is explained in chapter three. The experimental results are for both the BT and copper were measured and a bilinear fit was determined. The BT results are shown in Figure 30.

Reproduced with permission of the copyright owner. Further reproduction prohibited without permission.

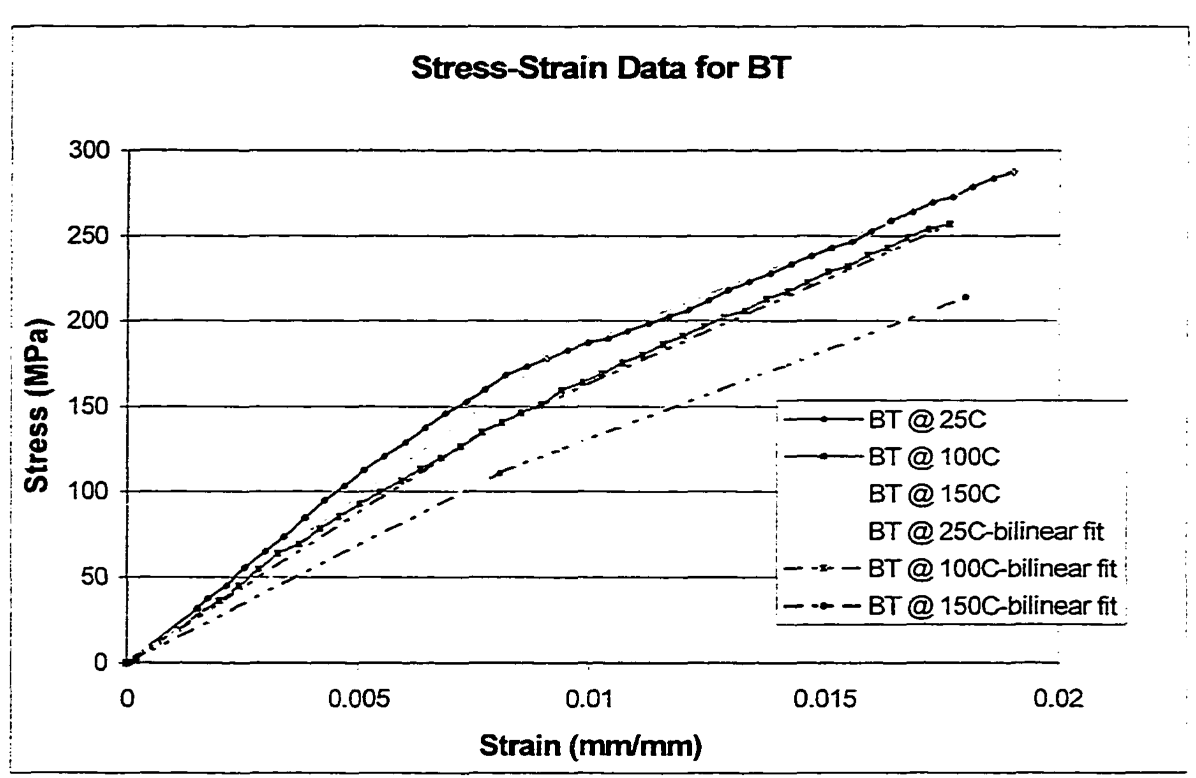

FIGURE 30. Experimental results and bilinear fit of BT resin.

The experimental measurements of the copper material followed similar procedure as stated in chapter three. The results and bilinear fit for each temperature are shown in Figure 31. Once all material properties were determined, input files were generated representing these materials and loaded into the finite element model.

Reproduced with permission of the copyright owner. Further reproduction prohibited without permission.

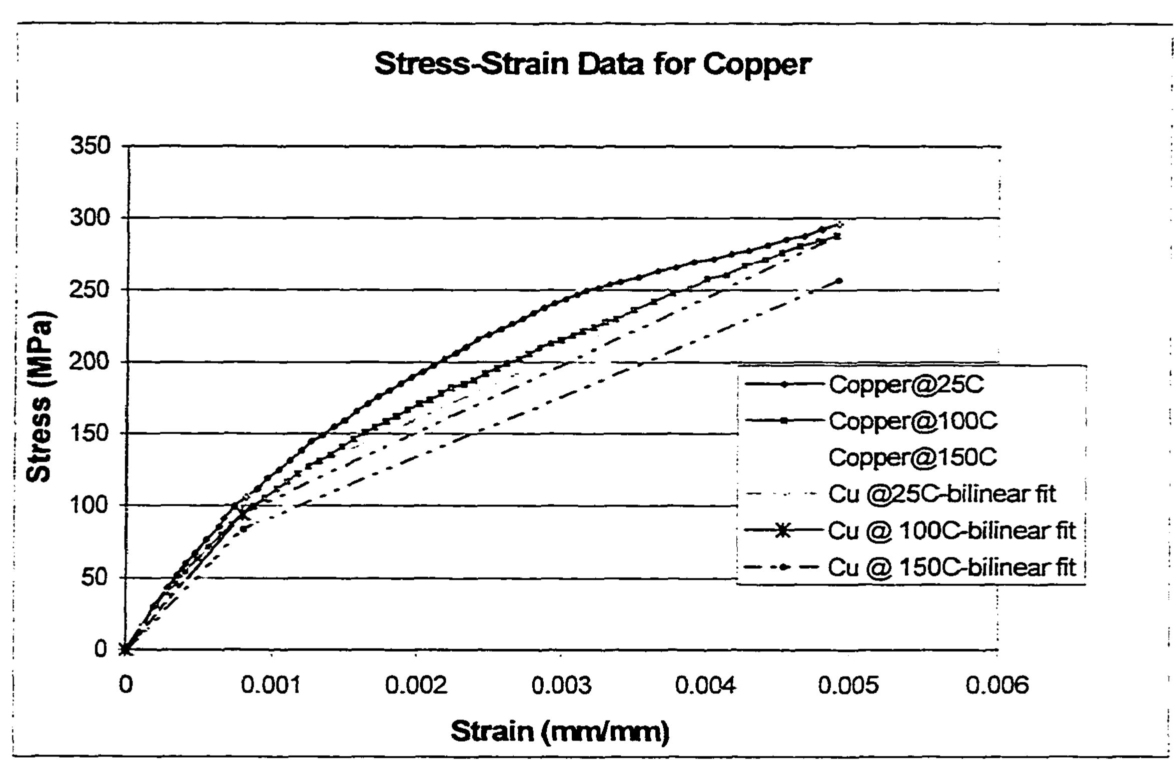

FIGURE 31. Experimental temperature dependent and bilinear fit of copper.

All other materials used in the finite element model were obtained using industry standard databases and the reference materials listed herein. Both measured properties and bilinear fit properties were used in the models and the results were compared as shown in chapter five.

Reproduced with permission of the copyright owner. Further reproduction prohibited without permission.

APPENDIX B

RELIABILITY MODELS FOR CREEP STRAIN ANALYSIS

Reproduced with permission of the copyright owner. Further reproduction prohibited without permission.

Relative life for low-cycle fatigue is determined by comparing the plastic creep deformation corresponding to each input level. If the life comparison is from a large cycle to a small cycle, the assumption that the plastic creep deformation is equal to the total deformation is conservative since the plastic creep deformation is a smaller fraction of the total for a small cycle. With this assumption in mind and taking the deformation as proportional to the thermal cycling range, the relative life for low-cycle fatigue is shown by:

$$n_{f_1} = \frac{1}{2}\left(\frac{\Delta\varepsilon_{c_1}}{2\varepsilon_f'}\right)^{\frac{1}{c}} \tag{B-1}$$

$$n_{f_2} = \frac{1}{2}\left(\frac{\Delta\varepsilon_{c_2}}{2\varepsilon_f'}\right)^{\frac{1}{c}} \tag{B-2}$$

Dividing the above equations:

$$\frac{n_{f_1}}{n_{f_2}} = \left(\frac{\Delta\varepsilon_{c_1}}{\Delta\varepsilon_{c_2}}\right)^{\frac{1}{c}} \approx \left(\frac{\Delta\varepsilon_{t_1}}{\Delta\varepsilon_{t_2}}\right)^{\frac{1}{c}} = \left(\frac{\Delta T_1}{\Delta T_2}\right)^{\frac{1}{c}} \tag{B-3}$$

where:

$n_{f1,2}$ = Mean Cycle to Fail at Level 1,2

$\Delta\varepsilon_{c1,2}$ = Creep Strain at Level 1,2

$2\varepsilon_{f'}$ = Fatigue Ductility Coefficient

c = Fatigue Ductility Exponent

$\Delta\varepsilon_{t1,2}$ = Total Strain at Level 1,2

$\Delta T_{1,2}$ = Thermal Cycle Range at Level 1,2

Reproduced with permission of the copyright owner. Further reproduction prohibited without permission.

Relative life for solder is similar to the generic low-cycle fatigue life comparison described above but since the fatigue ductility coefficient accounts for the relationship between plastic creep strain and total strain, it is no longer necessary to assume that plastic creep deformation equals total deformation. In addition, the life correction factor and temperature dependent ductility coefficient, c, make it necessary for the relative life to be based upon a specific number of cycles instead of a life ratio as shown in equation B-3.

With this known, the first step is to back-out the life correction factor from the reference cycles to fail to obtain an uncorrected cycles to fail shown by:

$$N_F = K_R\, K_L\, n_f \qquad \text{(B-4)}$$

$$K_L = \left(\frac{2500}{n_f}\right)^{\frac{1}{3}} \qquad (\text{for } n_f > 2500) \qquad \text{(B-5)}$$

$$K_L = 1 \qquad (\text{for } n_f < 2500) \qquad \text{(B-6)}$$

Considering reliability for test and evaluation environments:

$$n_{f_1} = \frac{N_{f_1}}{K_L} \qquad \text{(B-7)}$$

$$K_L = \left(\frac{2500}{N_{f1}}\right)^{\frac{1}{3}} \qquad (\text{for } N_{f1} > 2500) \qquad \text{(B-8)}$$

$$K_L = 1 \qquad (\text{for } N_{f1} < 2500) \qquad \text{(B-9)}$$

where:

K_R = Reliability Correction Factor

K_L = Life Correction Factor

N_F = Corrected Cycles to Fail

Reproduced with permission of the copyright owner. Further reproduction prohibited without permission.

n_{f1} = Uncorrected Cycles to Fail for Reference Environment

N_{f1} = Cycles to Fail for Reference Environment

Once the life correction factor is account for, the approach for relative life analysis is to use the temperature range to establish solder strain and use the solder strain to establish relative solder life. The relationship between life and solder strain is expressed in simplified form as:

$$n_f = \frac{1}{2}\left(\frac{\Delta\gamma}{2\varepsilon_f'}\right)^{\frac{1}{c}} \quad \text{(B-10)}$$

$$c = -0.442 - 6x10^{-4} T_{SJ} + 0.0174 \ln\left(1 + \frac{360}{t_D}\right) \quad \text{(B-11)}$$

$$\Delta\gamma = \frac{L_D}{hS}\left(\Delta\alpha\Delta T + \alpha_c \Delta T_c\right) + \Delta\alpha_{SM}\Delta T \quad \text{(B-12)}$$

where: n_f = Uncorrected Cycles to Fail

γ = Shear Strain

$2\varepsilon_f$ = Fatigue Ductility Coefficient

c = Fatigue Ductility Coefficient

T_{SJ} = Average Solder Temperature (0C)

t_D = Half-Cycle Dwell Time (min)

L_D = Diagonal Distance from Package Center

H = Solder Joint Height

S = Strain Factor

$\Delta\alpha$ = CTE Mismatch between Package and PWB

α_p = Package CTE

Reproduced with permission of the copyright owner. Further reproduction prohibited without permission.

ΔT_C = Temperature Rise of Package Due to Power

$\Delta\alpha_{SM}$ = Mismatch between Solder and Package

ΔT = Thermal Cycling Range

The relationship between the solder strain and temperature cycling range depends upon which terms from equation B-13 are considered. If the local temperature rise of the component due to power is very small, the following approach is used:

$$\Delta\gamma = \frac{L_D}{hS}\left(\Delta\alpha\Delta T + \alpha_c x 0\right) + \Delta\alpha_{SM}\Delta T \qquad \text{(B-13)}$$

Expressing equation B-13 as a proportionality and including the fatigue ductility coefficient in the proportionality constant:

$$\Delta\gamma \propto \Delta T \qquad \text{(B-14)}$$

$$n_f = \frac{1}{2}\left(\frac{\Delta T}{F}\right)^{\frac{1}{c}} \qquad \text{(B-15)}$$

$$F = \frac{\Delta T_2}{\left(2n_{f1}\right)^{c1}} \qquad \text{(B-16)}$$

$$n_{f2} = \frac{1}{2}\left(\frac{\Delta T_2}{F}\right)^{\frac{1}{c_2}} \qquad \text{(B-17)}$$

where: F = Proportionality Factor

$n_{f1,2}$ = Uncorrected Cycles to Fail for Temperature Range 1,2

$c_{1,2}$ = Fatigue Ductility Exponent for Temperature Range 1,2

$\Delta T_{1,2}$ = Thermal Cycling Range 1,2

Reproduced with permission of the copyright owner. Further reproduction prohibited without permission.

If the temperature rise of the component is not small enough to neglect, the relationship life can be determined if the solder-to-component mismatch is neglected and expansion rates of the applicable components are known:

$$\Delta\gamma = \frac{L_D}{hS}(\Delta\alpha\Delta T + \alpha_c\Delta T_c) + 0x\Delta T \qquad \text{(B-18)}$$

Expressing equation B-13 as a proportionality and including the fatigue ductility coefficient in the proportionality constant:

$$\Delta\gamma \propto \Delta\alpha\Delta T + \alpha_c\Delta T_c \qquad \text{(B-19)}$$

$$n_f = \frac{1}{2}\left(\frac{\Delta\alpha\Delta T + \alpha_c\Delta T_c}{F'}\right)^{\frac{1}{c}} \qquad \text{(B-20)}$$

$$F' = \frac{\Delta\alpha\Delta T_1 + \alpha_c\Delta T_{c1}}{(2n_{f1})^{c_1}} \qquad \text{(B-21)}$$

$$n_{f2} = \frac{1}{2}\left(\frac{\Delta\alpha\Delta T_2 + \alpha_{c2}\Delta T_c}{F'}\right)^{\frac{1}{c_2}} \qquad \text{(B-22)}$$

where: F' = Proportionality Factor

$n_{f1,2}$ = Uncorrected Cycles to Fail for Temperature Range 1,2

$c_{1,2}$ = Fatigue Ductility Exponent for Temperature Range 1,2

$\Delta T_{1,2}$ = Thermal Cycling Range 1,2

$\Delta\alpha$ = CTE mismatch between Component and Substrate

αc = Component CTE

$\Delta Tc_{1,2}$ = Temperature Rise of Component due to Power for Condition 1,2

Once the uncorrected cycles to fail for the proposed environment is determined, the life correction factor is used to determine the cycles to fail:

Reproduced with permission of the copyright owner. Further reproduction prohibited without permission.

$$K_L = \left(\frac{2500}{n_{f2}}\right)^{\frac{1}{3}} \quad \text{(for } n_{f2} > 2500\text{)} \tag{B-23}$$

$$K_L = 1 \quad \text{(for } n_{f2} < 2500\text{)} \tag{B-24}$$

Considering reliability for test and evaluation environments:

$$N_{f2} = K_L n_{f2} \tag{B-25}$$

where: K_L = Life Correction Factor

n_{f2} = Uncorrected Cycles to Fail for Proposed Environment

N_{f2} = Cycles to Fail for Proposed Environment

Since the life correction factor depends upon an absolute number of cycles and the fatigue ductility exponent varies with temperature, the acceleration factor between the environments is not scaleable. The following example is used to demonstrate the preceding equations and their use in determining the solder joint reliability of a package. Similar to the actual experiment, the device background heating is assumed to be zero so the shear strain equation B-13 is chosen and expanded to account for both X and Y direction of the package. The package size is assumed to be 5.0mm in both X and Y direction and the temperature range is from –55C to 125C with a dwell of 10 minutes.

$$\Delta\gamma = \frac{\sqrt{(L_x \Delta\alpha_x \Delta T)^2 + (L_y \Delta\alpha_y \Delta T)^2}}{2hS} + \Delta\alpha_{SM} \Delta T$$

$$\Delta\gamma = \frac{\sqrt{(5*3*180)^2 + (5*3*180)^2}}{2*0.050*6.56} + 22.3*180$$

$\Delta\gamma$ = 9834 ppm = 0.00983%

Solving for the fatigue ductility exponent from equation A2-11

Reproduced with permission of the copyright owner. Further reproduction prohibited without permission.

$$c = -0.442 - 6x10^{-4} * 35 + 0.0174 \ln\left(1 + \frac{360}{10}\right)$$

c = -0.40017

Plugging into equation A2-10,

$$n_f = \frac{1}{2}\left(\frac{.00983}{0.65}\right)^{\frac{1}{-0.40017}} = 17695 \text{ cycles}$$

Since $n_f > 2500$ cycles, the life correction factor (K_l) is found as:

$$K_L = \left(\frac{2500}{17695}\right)^{\frac{1}{3}} = 0.5208$$

The reliability correction factor for 1% failure is found as:

$$K_r = \alpha'(-\ln(1-F))^{\frac{1}{\beta}} \qquad \text{(B-26)}$$

F = Cummulative Failure Probability = 1% = 0.01

α' = Weibull Scale Parameter = 1.096

β = Weibull Shape Parameter = 4.00

$K_r = 0.347$

With all required values known, the corrected thermal cycle life prediction is determined using the product of the uncorrected prediction and the two correction factors.

$N_f = K_r * Kl * n_f = 0.347 * 0.5208 * 1074.33$

$N_f = 3198$ cycles

For first order estimates on the solder joint reliability, $\Delta\gamma$ can be estimated as previously shown. However, for a more accurate prediction, $\Delta\gamma$ is measured using ESPI

Reproduced with permission of the copyright owner. Further reproduction prohibited without permission.

techniques as well as numerically solved for using FEM. From the finite element results, using the experimental material properties, $\Delta\gamma$ is equal to 0.0068 mm/mm and plugging into equation B-10:

$$n_f = \frac{1}{2}\left(\frac{0.00682}{0.65}\right)^{\frac{1}{-0.40017}} = 44118$$

$$K_L = \left(\frac{2500}{xxx}\right)^{\frac{1}{3}} = 0.384$$

$$K_r = 0.347$$

$N_f = 5880$ cycles

Reproduced with permission of the copyright owner. Further reproduction prohibited without permission.

APPENDIX C

ANSYS INPUT DECK FILES

Reproduced with permission of the copyright owner. Further reproduction prohibited without permission.

start.inp

```
/batch
/com  *****************************************************************
/com
/com  This model represents a 5mmx5mm LGA package with a 2mmx2mm
/com  silicon die.  Implicit creep analysis using the Sinh hyperbolic
/com  law for eutectic solder.  Thermal cycling of the package from
/com  -55C to 125C with 10 minute dwells.  This input deck works with
/com  ANSYS 5.6 or later.
/com  *****************************************************************

/com  Argument 1: lumped package size (mm); 5mm
/com  Argument 2: silicon die size (mm); 2mm
/com  Argument 3: PWB size (mm); 7mm

/config,nres,10000       ! maximum number of saved result steps to 10000
model,5.0,2.0,7.0
/input,mat,inp
/input,mesh,inp
/input,solve_3x,inp
```

exit

Reproduced with permission of the copyright owner. Further reproduction prohibited without permission.

model.inp

```
/com  ******************************************************************
/com
/com  2-D, plane strain model of LGA
/com  Model file sets up array and generates areas for meshing
/com
/com   *****************************************************************

/prep7

/com  Define arguments
packsize       = arg1
sisize         = arg2
pwbsize        = arg3

/com  Dimension Arrays
*dim,x,,50
*dim,y,,50
*dim,z,,50
*dim,kpt,,50

/com  Define parameters (units are input in mm)
/com  Thickness of materials
sldrthk = 0.050          ! solder joint standoff
cuthk = 0.020            ! thickness of copper pad
sithk = 0.330            ! thickness of silicon die
moldthk = 0.890          ! thickness of mold cap
pcbthk = 0.200           ! thickness of pcb substrate
pwbthk  = 0.600          ! thickness of pwb

/com  Solder joint details
cupcbw  = 0.500          ! width of copper pad on RFLGA package
sldrw   = 0.300          ! wicth of solder joint
cupwbw  = 0.700          ! width of copper pad on PWB
ctrpad  = 2.0            ! solder center pad diameter

/com   Define Keypoints (units are converted to mm)

tol     = 0.0001         ! tolerance for geometry location

x(1)    = 0.0
x(2)  = sisize/2
x(3)  = packsize/2-cupcbw
x(4)  = packsize/2-sldrw
x(5)  = packsize/2
x(6)  = x(3)+cupwbw
x(7)  = pwbsize/2

y(1)  = 0.0
y(2)  = pwbthk
y(3)  = y(2)+cuthk
y(4)  = y(3)+sldrthk
y(5)  = y(4)+cuthk
y(6)  = y(5)+pcbthk
```


Reproduced with permission of the copyright owner. Further reproduction prohibited without permission.

```
y(7)   = y(6)+sithk
y(8)   = y(6)+moldthk
/com  Build Geometry

/com pwb
*do,i,1,6
rectangle,x(i),x(i+1),y(1),y(2)
*enddo

/com center pad
*do,j,2,4
rectangle,x(1),x(2),y(j),y(j+1)
*enddo

/com solder joint
*do,i,3,5
rectangle,x(i),x(i+1),y(2),y(3)
*enddo
rectangle,x(4),x(5),y(3),y(4)
*do,i,3,4
rectangle,x(i),x(i+1),y(4),y(5)
*enddo

/com RFLGA package
*do,j,5,7
*do,i,1,4
rectangle,x(i),x(i+1),y(j),y(j+1)
*enddo
*enddo

asel,all
aglue,all

asel,all
nummrg,all
```


Reproduced with permission of the copyright owner. Further reproduction prohibited without permission.

mat.inp

```
/com  Material Properties : 1) Silicon , 2) eutectic solder ,
/com                          3) PWB, 4) BT, 5) mold, 6) copper

/com  Material 1 - Si
modsi   = 188e3      ! modulus of Si (from CINDAS) (units in MPa)
poissi  = 0.30
ctesi   = 2.7e-6     ! units in /C
!mp,reft,1,tciba
mp,ex,1,modsi
mp,nuxy,1,poissi
mp,alpx,1,ctesi


/com  Material 2 - 63Sn/37Pb  (eutectic) solder
/com       from CINDAS database
poispbsn = 0.35       ! from 63Sn/37Pb solder - CINDAS
ctepbsn  = 29.1e-6    ! units in /C (from 63/37 PbSn solder - CINDAS)
mp,nuxy,2,poispbsn
mp,alpx,2,ctepbsn
mp,ex,2,40300*0.6

/com  Creep strain-rate dependent properties,63/37 SnPb solder from RSC
tb,creep,2,1,100,8     ! 8 signifies hyperbolic sine law
tbtemp,307             ! average temperature (-55 and 125)
tbdata,1,1300000,2.4,0.102,9116.779


/com  Material 3 - FR-4 PWB
modfr4   = 14e3        ! MPa
poisfr4  = 0.3         ! approximate (no data available)
ctefr4   = 16.0e-6     ! units in /C
mp,ex,3,modfr4
mp,nuxy,3,poisfr4
mp,alpx,3,ctefr4


/com  Material 4 - BT Resin
poisbt   = 0.15        ! avg. of 0.14 (x-dir) and 0.16 (y-dir)
ctebt    = 16.2e-6
mp,nuxy,4,poisbt
mp,alpx,4,ctebt

/com bilinear properties of BT, fit from measurements
tb,miso,4,3,65
/input,btbi25,inp
/input,btbi100,inp
/input,btbi150,inp
mptemp

/com   elastic-plastic properties, directly from measurements
tb,miso,4,3,65
/input,bt25,inp
/input,bt100,inp
```


Reproduced with permission of the copyright owner. Further reproduction prohibited without permission.

```
/input,bt150,inp
mptemp


/com  Material 5 - Sumitomo EME7720S  (for BGA's; from vendor)
poissumi = 0.25        ! from Anam's Plaskon SMTB1 mold compound
ctesumi  = 13.0e-6     ! CTE (ppm/C) below Tg=190C
mp,nuxy,5,poissumi
mp,alpx,5,ctesumi
mptemp,1,25,240
mpdata,ex,5,1,19.6e3,2156
mptemp


/com  Material 6 - Copper
poisbt = 0.15          ! avg. of 0.14 (x-dir) and 0.16 (y-dir)
ctebt = 21.2e-6
mp,nuxy,6,poisbt
mp,alpx,6,ctebt

/com bilinear properties of Copper, fit from measurements
tb,miso,6,3,65
/input,cubi25,inp
/input,cubi100,inp
/input,cubi150,inp
mptemp

/com  elastic-plastic properties directly from measurements
tb,miso,6,3,65
/input,cu25,inp
/input,cu100,inp
/input,cu150,inp
mptemp
```


Reproduced with permission of the copyright owner. Further reproduction prohibited without permission.

mesh.inp

```
/com   ****************************************************************
/com
/com  Mesh input file using Plane183 plane strain elements
/com
/com   ****************************************************************

/com  Define Element Type
/com  2-D 8-node plane element, UX,UY - plane strain
et,1,plane183,,,2,

/com  Assign Materials to areas
/com  Si
asel,s,loc,y,y(6),y(7)
asel,r,loc,x,x(1),x(2)
aatt,1,,1

/com  Solder
asel,s,loc,y,y(3),y(4)
aatt,2,,1

/com  PWB
asel,s,loc,y,y(1),y(2)
aatt,3,,1

/com  BT
asel,s,loc,y,y(5),y(6)
aatt,4,,1

/com  Copper
asel,s,loc,y,y(2),y(3)
asel,a,loc,y,y(4),y(5)
aatt,6,,1

/com  Mold
allsel
asel,u,mat,,1
asel,u,mat,,2
asel,u,mat,,3
asel,u,mat,,4
asel,u,mat,,6
aatt,5,,1

/com  Mesh model, define global element size
lsize1 = 0.02
lsize2 = 0.05

/com  refined mesh
eshape,2,0

esize,lsize1      ! define element size for chosen areas

/com  Mesh copper pad of solder joint
lsel,s,loc,y,y(2)+tol,y(3)-tol
```


Reproduced with permission of the copyright owner. Further reproduction prohibited without permission.

```
lesize,all,,,6,-1,,
lsel,s,loc,y,y(4)+tol,y(5)-tol
lesize,all,,,6,-1,,

/com  Mesh solder joint
lsel,s,loc,y,y(3)+tol,y(4)-tol
lesize,all,,,14,-4,,

/com  Mesh PWB
lsel,s,loc,x,x(1)+tol,x(2)-tol
lesize,all,,,35,1,,

lsel,s,loc,y,y(1)+tol,y(2)-tol
lsel,r,loc,x,x(1)+tol,x(7)
lesize,all,,,19,0.2,,

lsel,s,loc,x,x(3)+tol,x(4)-tol
lsel,r,loc,y,y(1),y(2)
lesize,all,,,13,.2,,
lsel,s,loc,x,x(3)+tol,x(4)-tol
lsel,r,loc,y,y(6),y(8)
lesize,all,,,13,.2,,
lsel,s,loc,x,x(3)+tol,x(4)-tol
lsel,r,loc,y,y(3),y(5)
lesize,all,,,13,5,,

lsel,s,loc,x,x(4)+tol,x(5)-tol
lesize,all,,,21,-5,,
lsel,s,loc,x,x(5)+tol,x(6)-tol
lesize,all,,,12,6,,

/com Mesh lumped package
lsel,s,loc,y,y(5)+tol,y(6)-tol
lsel,r,loc,x,x(1)+tol,x(5)
lesize,all,,,14,7,,

esize,lsize2       ! define element size for chosen areas
asel,all
lsel,u,loc,x,x(3),x(5)
amesh,all


/com  Sort model to minimize wavefront (reduce calculation time)

waves


finish
```


Reproduced with permission of the copyright owner. Further reproduction prohibited without permission.

solve 3x.inp

```
/com  Solve model
/solu

/com  nonlinear analysis solution options/controls
/com  thermal cycle three times, -55C to 125C w/ 10min dwells

allsel

esel,s,mat,,2             ! select solder elements
cm,solder,elem            ! set solder elements as component for data
save
outres,esol,2,solder      ! save results of solder every 2 seconds

cnvtol,f,,,,-1            ! set min force convergence to off

allsel

/com  newton-raphson method has to be set explicitly(full)
antype,static,new         ! new static analysis
nlgeom,on                 ! set non-linear analysis on
nropt,auto,,off
rate,on                   ! specifies creep strain rate  is used
                          ! in the solution of a load step
autots,on                 ! activate auto time step
deltim,2,1.5,60,on        ! set time step, start,min,max seconds
eqslv,pcg,1e-6
crplim,0.75,on            ! creep criteria for auto time step = 75%

/com  define boundary conditions for plane strain analysis
/com  symmetry constraints
nsel,s,loc,x,x(1)-tol,x(1)+tol
d,all,ux,0
nsel,s,loc,x,x(1)-tol,x(1)+tol
nsel,r,loc,y,y(1)-tol,y(1)+tol
d,all,uy,0.

allsel

/com  define load steps

/com cycle definition
hightemp = 125+273        ! high cycle temp
highramp = 1200           ! low to high ramp (sec) = 20min
highdwel = 600            ! high dwell (sec) = 10min

lowtemp = -55+273         ! low cycle temp
lowramp = 1200            ! high to low ramp (sec) = 20min
lowdwel = 600
cycle = 3600              ! total time for each cycle

tref, hightemp

/com THERMAL CYCLE #1
```


Reproduced with permission of the copyright owner. Further reproduction prohibited without permission.

```
/com COOL TO -55C
bfe,all,temp,,lowtemp    ! apply temp to nodes
kbc,0                    ! linearly ramp temps
time,lowramp             ! set time at end of step
solve                    ! solve load step
save                     ! save data

/com DWELL AT -55C FOR 10 MINUTES
bfe,all,temp,,lowtemp    ! apply temp to nodes
kbc,1                    ! maintain temps
time,lowramp+lowdwel     ! set time at end of step
solve                    ! solve load step
save                     ! save data

/com HEAT TO 125C
bfe,all,temp,,hightemp   ! apply temp to nodes
kbc,0                    ! linearly ramp temps
time,lowramp+lowdwel+highramp
solve
save

/com DWELL AT 125C
bfe,all,temp,,hightemp   ! apply temp to nodes
kbc,1                    ! maintain temps
time,lowramp+lowdwel+highramp+highdwel
solve
save


/com THERMAL CYCLE #2
/com COOL TO -55C
bfe,all,temp,,lowtemp    ! apply temp to nodes
kbc,0                    ! linearly ramp temps
time,cycle+lowramp       ! set time at end of step
solve                    ! solve load step
save                     ! save data

/com DWELL AT -55C FOR 10 MINUTES
bfe,all,temp,,lowtemp    ! apply temp to nodes
kbc,1                    ! maintain temps
time,cycle+lowramp+lowdwel     ! set time at end of step
solve                    ! solve load step
save                     ! save data

/com HEAT TO 125C
bfe,all,temp,,hightemp   ! apply temp to nodes
kbc,0                    ! linearly ramp temps
time,cycle+lowramp+lowdwel+highramp
solve
save

/com DWELL AT 125C
bfe,all,temp,,hightemp   ! apply temp to nodes
kbc,1                    ! maintain temps
time,cycle+lowramp+lowdwel+highramp+highdwel
```


Reproduced with permission of the copyright owner. Further reproduction prohibited without permission.

```
solve
save


/com THERMAL CYCLE #3
/com COOL TO -55C
bfe,all,temp,,lowtemp    ! apply temp to nodes
kbc,0                    ! linearly ramp temps
time,2*cycle+lowramp     ! set time at end of step
solve                    ! solve load step
save                     ! save data

/com DWELL AT -55C FOR 10 MINUTES
bfe,all,temp,,lowtemp    ! apply temp to nodes
kbc,1                    ! maintain temps
time,2*cycle+lowramp+lowdwel  ! set time at end of step
solve                    ! solve load step
save                     ! save data

/com HEAT TO 125C
bfe,all,temp,,hightemp   ! apply temp to nodes
kbc,0                    ! linearly ramp temps
time,2*cycle+lowramp+lowdwel+highramp
solve
save

/com DWELL AT 125C
bfe,all,temp,,hightemp   ! apply temp to nodes
kbc,1                    ! maintain temps
time,2*cycle+lowramp+lowdwel+highramp+highdwel
solve
save


finish
```


Reproduced with permission of the copyright owner. Further reproduction prohibited without permission.

crxy.inp - script file to pull results of time for multiple elements

```
/com, DESCRIPTION & MACRO REVISION:
/com, This macro computes the average shear stress (S-XY) and creep
/com, shear strain (EPCL-XY) for a selected set of elements over time.

! USAGE OF MACRO:
!    "crxy" (no arguments needed)
!
! OUTPUT OF MACRO:
! Places average shear stress into SXY POST26 variable
! Places average creep shear strain into EPCR POST26 variable
!
finish
/pmacro
*MSG,UI
After closing this dialog box, select the elements you wish to average.

esel,s,p
nsle,s,all
*get,nelemsel,elem,0,count
*get,celemn,elem,0,num,min
/post26
esol,2,celemn,,s,xy,sxy

store,new
*get,nsets,vari,0,nsets
finish
/post1
*dim,rarray,array,nelemsel,3,nsets
*dim,ararray,array,nsets,3

set,last
*do,index1,1,nsets,1
set,next
etable,sxy,s,xy
etable,epcr,epcr,xy
etable,epel,epel,xy

*get,celemn,elem,0,num,min
*do,index2,1,nelemsel,1
*get,rarray(index2,1,index1),etab,1,elem,celemn
*get,rarray(index2,2,index1),etab,2,elem,celemn
*get,rarray(index2,3,index1),etab,3,elem,celemn

celemn=elnext(celemn)
*enddo
*vscfun,ararray(index1,1),mean,rarray(1,1,index1)
*vscfun,ararray(index1,2),mean,rarray(1,2,index1)
*vscfun,ararray(index1,3),mean,rarray(1,3,index1)

*enddo
finish
/post26
*get,celemn,elem,0,num,min
```


Reproduced with permission of the copyright owner. Further reproduction prohibited without permission.

```
esol,2,celemn,,s,xy,SXY
vput,ararray(1,1),2
esol,3,celemn,,epcr,xy,EPCR
vput,ararray(1,2),3
esol,4,celemn,,epel,xy,EPEL
vput,ararray(1,3),4

plvar,3,4                       ! Plot epsilon and elastic xy
```


Reproduced with permission of the copyright owner. Further reproduction prohibited without permission.

bt25.inp

```
!  BT at 25C
tbtemp,298
tbpt,,0,0
tbpt,,0.0015,31.80
tbpt,,0.00172,37.62
tbpt,,0.00213,45.14
tbpt,,0.00255,55.74
tbpt,,0.00299,65.32
tbpt,,0.00339,73.53
tbpt,,0.00383,84.81
tbpt,,0.00425,94.73
tbpt,,0.0047,103.28
tbpt,,0.00512,112.52
tbpt,,0.00556,120.73
tbpt,,0.00601,128.93
tbpt,,0.00644,137.48
tbpt,,0.00687,146.03
tbpt,,0.00732,152.88
tbpt,,0.00773,160.06
tbpt,,0.00817,168.27
tbpt,,0.00863,173.05
tbpt,,0.00907,177.84
tbpt,,0.00953,182.63
tbpt,,0.00997,187.08
tbpt,,0.01039,189.47
tbpt,,0.0108,193.92
tbpt,,0.01125,198.36
tbpt,,0.01168,202.47
tbpt,,0.0121,206.23
tbpt,,0.01252,212.04
tbpt,,0.01294,217.86
tbpt,,0.01338,222.65
tbpt,,0.01383,227.78
tbpt,,0.01426,233.25
tbpt,,0.01469,238.04
tbpt,,0.01513,242.82
tbpt,,0.01558,246.59
tbpt,,0.01599,252.74
tbpt,,0.0164,258.90
tbpt,,0.01688,264.03
tbpt,,0.0173,269.50
tbpt,,0.01774,272.58
tbpt,,0.01816,278.74
tbpt,,0.01861,283.87
tbpt,,0.01904,287.63
```


Reproduced with permission of the copyright owner. Further reproduction prohibited without permission.

<u>bt100.inp</u>

```
! BT at 100C
tbtemp,373
tbpt,,0,0
tbpt,,0.00007,0.64
tbpt,,0.00005,0.32
tbpt,,0.00022,2.89
tbpt,,0.00067,12.21
tbpt,,0.0011,19.60
tbpt,,0.00152,28.91
tbpt,,0.00197,36.30
tbpt,,0.00241,44.65
tbpt,,0.00285,54.61
tbpt,,0.00326,63.93
tbpt,,0.00371,69.39
tbpt,,0.00415,78.39
tbpt,,0.00457,85.45
tbpt,,0.00503,92.52
tbpt,,0.00547,99.59
tbpt,,0.00591,106.34
tbpt,,0.00634,113.40
tbpt,,0.00678,119.83
tbpt,,0.0072,126.58
tbpt,,0.00766,134.93
tbpt,,0.00809,140.39
tbpt,,0.00852,146.17
tbpt,,0.00895,150.99
tbpt,,0.00938,159.34
tbpt,,0.00984,163.84
tbpt,,0.01025,168.98
tbpt,,0.01069,175.41
tbpt,,0.01112,179.90
tbpt,,0.01156,186.33
tbpt,,0.01199,191.15
tbpt,,0.01243,196.61
tbpt,,0.01285,202.07
tbpt,,0.01329,205.93
tbpt,,0.01374,212.67
tbpt,,0.01419,217.17
tbpt,,0.01461,222.31
tbpt,,0.01505,228.74
tbpt,,0.01548,231.95
tbpt,,0.01591,238.69
tbpt,,0.01634,242.87
tbpt,,0.01677,248.97
tbpt,,0.01722,253.79
tbpt,,0.01767,257.01
```


Reproduced with permission of the copyright owner. Further reproduction prohibited without permission.

bt150.inp

```
! BT at 150C
tbtemp,423
tbpt,,0,0
tbpt,,0.00043,7.99
tbpt,,0.0004,9.27
tbpt,,0.00065,10.55
tbpt,,0.00106,18.22
tbpt,,0.00149,24.93
tbpt,,0.00194,31.01
tbpt,,0.00237,40.92
tbpt,,0.00282,45.07
tbpt,,0.00326,52.11
tbpt,,0.00364,57.86
tbpt,,0.0041,64.57
tbpt,,0.00457,69.69
tbpt,,0.00499,75.12
tbpt,,0.00543,80.56
tbpt,,0.00589,85.99
tbpt,,0.00629,91.11
tbpt,,0.00672,96.22
tbpt,,0.0072,99.74
tbpt,,0.0076,105.17
tbpt,,0.00804,110.93
tbpt,,0.0085,115.40
tbpt,,0.00892,122.76
tbpt,,0.00935,125.95
tbpt,,0.00979,129.47
tbpt,,0.01022,134.90
tbpt,,0.01067,139.38
tbpt,,0.01108,142.58
tbpt,,0.0115,148.01
tbpt,,0.01193,152.80
tbpt,,0.01238,156.00
tbpt,,0.01282,163.67
tbpt,,0.01324,166.55
tbpt,,0.01369,169.43
tbpt,,0.01409,175.18
tbpt,,0.01455,179.02
tbpt,,0.01498,182.85
tbpt,,0.0154,187.97
tbpt,,0.01586,191.49
tbpt,,0.0163,196.28
tbpt,,0.01671,200.12
tbpt,,0.01716,204.91
tbpt,,0.0176,207.47
tbpt,,0.01802,213.86
```


Reproduced with permission of the copyright owner. Further reproduction prohibited without permission.

btbi25.inp

```
!    Bilinear model of BT at 25C
tbtemp,298
tbpt,,0,0
tbpt,,0.00907,177.84
tbpt,,0.01904,287.63
```

btbi100.inp

```
!    bilinear model of BT at 100C
tbtemp,373
tbpt,,0,0
tbpt,,0.00766,134.93
tbpt,,0.01767,257.01
```

btbi150.inp

```
!    Bilinear model of BT at 150C
tbtemp,423
tbpt,,0,0
tbpt,,0.00804,110.93
tbpt,,0.01802,213.86
```


Reproduced with permission of the copyright owner. Further reproduction prohibited without permission.

cu25.inp

```
! Copper at 25C
tbtemp,298
tbpt,,0,0.00
tbpt,,0.000191233,30.23
tbpt,,0.000285378,43.00
tbpt,,0.000350103,51.86
tbpt,,0.000406002,59.67
tbpt,,0.000470727,66.97
tbpt,,0.00054722,76.35
tbpt,,0.000635481,85.47
tbpt,,0.000667843,91.20
tbpt,,0.000741395,99.54
tbpt,,0.00082083,105.80
tbpt,,0.000897323,111.79
tbpt,,0.000967932,119.35
tbpt,,0.001047367,125.08
tbpt,,0.00112386,131.33
tbpt,,0.001203295,138.37
tbpt,,0.001270962,144.62
tbpt,,0.001347455,149.05
tbpt,,0.00142689,155.05
tbpt,,0.001500441,159.22
tbpt,,0.001579876,165.73
tbpt,,0.001659312,171.20
tbpt,,0.001732863,175.89
tbpt,,0.001806414,180.06
tbpt,,0.001882907,185.01
tbpt,,0.0019594,189.44
tbpt,,0.002032951,193.09
tbpt,,0.002109444,197.78
tbpt,,0.002185937,202.21
tbpt,,0.002268314,206.12
tbpt,,0.002338923,210.29
tbpt,,0.002415416,215.50
tbpt,,0.002488967,218.63
tbpt,,0.002571345,222.54
tbpt,,0.002644896,226.19
tbpt,,0.002718447,229.83
tbpt,,0.002791998,234.00
tbpt,,0.002868491,237.39
tbpt,,0.002942042,240.78
tbpt,,0.003018535,243.64
tbpt,,0.00309797,246.77
tbpt,,0.003165637,249.38
tbpt,,0.003250956,251.46
tbpt,,0.003327449,253.55
tbpt,,0.003403942,255.63
tbpt,,0.00353045,259.02
tbpt,,0.0036599,263.19
tbpt,,0.003783466,265.53
tbpt,,0.003909974,269.44
tbpt,,0.004045307,271.53
tbpt,,0.004165931,274.91
```


Reproduced with permission of the copyright owner. Further reproduction prohibited without permission.

```
tbpt,,0.004292439,277.52
tbpt,,0.004424831,281.17
```

cu100.inp

```
! copper at 100C
tbtemp,373
tbpt,,0,0
tbpt,,0.00011474,15.90
tbpt,,0.00011474,15.90
tbpt,,0.000208885,30.75
tbpt,,0.000279494,39.87
tbpt,,0.000344219,46.38
tbpt,,0.00040306,54.46
tbpt,,0.000488379,63.58
tbpt,,0.000567814,71.40
tbpt,,0.000650191,80.00
tbpt,,0.000723742,86.77
tbpt,,0.000797293,94.33
tbpt,,0.000873786,99.54
tbpt,,0.000947337,105.54
tbpt,,0.001026773,111.53
tbpt,,0.001103266,116.48
tbpt,,0.001173875,121.95
tbpt,,0.00125331,127.16
tbpt,,0.001326861,131.07
tbpt,,0.001406296,135.24
tbpt,,0.001479847,140.97
tbpt,,0.001559282,146.19
tbpt,,0.001635775,150.88
tbpt,,0.001706384,154.53
tbpt,,0.001785819,158.69
tbpt,,0.001856428,162.34
tbpt,,0.001935863,166.77
tbpt,,0.002015299,170.94
tbpt,,0.002085908,173.55
tbpt,,0.002162401,177.98
tbpt,,0.002235952,182.41
tbpt,,0.002318329,184.75
tbpt,,0.002388938,187.36
tbpt,,0.002468373,192.05
tbpt,,0.002541924,195.70
tbpt,,0.002609591,199.08
tbpt,,0.00269491,202.21
tbpt,,0.002762577,205.86
tbpt,,0.002842012,209.77
tbpt,,0.002921447,212.37
tbpt,,0.002989114,214.98
tbpt,,0.003071492,218.11
tbpt,,0.003142101,221.23
tbpt,,0.003218594,223.84
tbpt,,0.003295087,227.75
tbpt,,0.00337158,229.57
tbpt,,0.003498088,236.09
tbpt,,0.003627538,242.08
tbpt,,0.003756987,247.81
```


Reproduced with permission of the copyright owner. Further reproduction prohibited without permission.

```
tbpt,,0.003883495,250.68
tbpt,,0.004001177,257.98
tbpt,,0.004136511,260.58
tbpt,,0.004263019,266.84
```


Reproduced with permission of the copyright owner. Further reproduction prohibited without permission.

cu150.inp

```
! Copper at 150C
tbtemp,423
tbpt,,0,0
tbpt,,0.000117682,16.55
tbpt,,0.000126508,15.51
tbpt,,0.000220653,26.63
tbpt,,0.00028832,35.16
tbpt,,0.000353045,40.85
tbpt,,0.000414828,47.31
tbpt,,0.000494263,54.55
tbpt,,0.000579582,62.56
tbpt,,0.000656075,70.58
tbpt,,0.000723742,76.27
tbpt,,0.000803177,83.51
tbpt,,0.000885555,87.64
tbpt,,0.000967932,92.04
tbpt,,0.001032657,97.72
tbpt,,0.001112092,101.86
tbpt,,0.001185643,106.26
tbpt,,0.001259194,111.43
tbpt,,0.001341571,116.08
tbpt,,0.00141218,121.25
tbpt,,0.001485731,125.39
tbpt,,0.001565166,128.23
tbpt,,0.001650485,132.11
tbpt,,0.001721094,136.25
tbpt,,0.001797588,140.38
tbpt,,0.001868197,144.00
tbpt,,0.001947632,146.59
tbpt,,0.002018241,150.46
tbpt,,0.00208885,154.34
tbpt,,0.002165343,157.70
tbpt,,0.002241836,160.81
tbpt,,0.002333039,162.62
tbpt,,0.002397764,166.49
tbpt,,0.002474257,169.34
tbpt,,0.00255075,172.96
tbpt,,0.002627243,175.28
tbpt,,0.002697852,177.87
tbpt,,0.002768461,182.52
tbpt,,0.002850838,185.37
tbpt,,0.0029391,187.69
tbpt,,0.003006767,190.02
tbpt,,0.003077376,194.41
tbpt,,0.003147985,196.48
tbpt,,0.003233304,198.55
tbpt,,0.003303913,201.40
tbpt,,0.003377464,204.76
tbpt,,0.003503972,209.41
tbpt,,0.003639306,214.58
tbpt,,0.003765813,218.46
tbpt,,0.003892321,222.59
tbpt,,0.004021771,226.73
```


Reproduced with permission of the copyright owner. Further reproduction prohibited without permission.

```
tbpt,,0.004148279,232.16
tbpt,,0.004277729,236.81
```

cubi25.inp

```
! Bilinear model of Copper at 25C
tbtemp,298
tbpt,,0,0.00
tbpt,,0.00082083,105.80
tbpt,,0.00492792,296.28
```

cubi100.inp

```
! Bilinear model of copper at 100C
tbtemp,373
tbpt,,0,0
tbpt,,0.000797293,94.33
tbpt,,0.004907326,287.94
```

cubi150.inp

```
! Bilinear model of Copper at 150C
tbtemp,423
tbpt,,0,0
tbpt,,0.000803177,83.51
tbpt,,0.004924978,256.98
```


Reproduced with permission of the copyright owner. Further reproduction prohibited without permission.

BIBLIOGRAPHY

Reproduced with permission of the copyright owner. Further reproduction prohibited without permission.

BIBLIOGRAPHY LIST

1. Lapedes, D. ed. McGraw-Hill Dictionary of Scientific and Technical Terms. Second Edition, McGraw-Hill, 1978.

2. McKeown, S. Mechanical Analysis of Electronic Packaging Systems. First Edition, Marcel Dekker, 1999.

3. Pecht, M. Electronic Packaging Materials and Their Properties, CRC Press, 1999.

4. Tummala, R., and Rymaszewski, E. Microelectronics Packaging Handbook, First Edition, Wiley, 1989.

5. Lee, S. and Kim J. "A Mechanistic Model for Fatigue Life Prediction of Solder Joints for Electronic Packages," International Journal of Fatigue, 19 (1), 1997.

6. Pecht, M. Electronic Packaging Materials and Their Properties, CRC Press, 1999.

7. Chen, B. Shi, L., Zou, D., and Liu, Sheng. "Moiré Interferometer Assist in Electronic Packaging Development," Journal of Advanced Packaging, Vol. 16, September 1999.

8. Tyson, J. "Non-contact Full-field Strain Measurement with 3-D ESPI," Journal of Machine Sensing, Vol. 23, February 2000.

9. Shih, Y.S., Yeh, Z.F., and Yeh, H.Y. A Study of Non-linear Thermal Constitutive Model of a Special Plastic Material, PTFE.

10. Timoshenko, S.P., and Gere, J.M. Theory of Elastic Stability, Second Edition, McGraw-Hill, 1961.

11. Kohnke, P. ANSYS Theory Reference, Release 5.3, Seventh Edition, ANSYS Inc., Houston PA; 1996.

12. Ibid.

Reproduced with permission of the copyright owner. Further reproduction prohibited without permission.